Chapter 4

Testing the structural and geomechanical processes in the formation of the Century (Zn-Pb-Ag) Deposit

Acknowledgement of Contributions

Contributions made to this chapter involved:

L. Feltrin – 3D Structural Modelling, Century data and review

Dr. J. G. McLellan – Geomechanical Modelling

Dr. D. R. W. Foster – Mount Isa Time Space Plot

L. Feltrin – 70% (p. 1-24), 90% (p.25-43), 10% (p. 44-76), 60% (p.77-80)

J. G. McLellan – 30% (p. 1-24), 10% (p. 25-43), 90% (p. 44-76), 40% (p. 77-80)

N.H.S. Oliver – normal supervisory contributions

Abstract

The Century zinc deposit is one of the giant Mesoproterozoic Zn-Pb-Ag deposits of the Northern Australian Zinc Belt. There is substantial controversy regarding the genesis of this deposit. Previous workers proposed a timing for the emplacement of the Century mineralisation as early diagenetic to syn-tectonic. In this work we present one of the first applications of 3D structural modelling combined with coupled mechanical and fluid flow modelling which aims to address ore genesis using computer simulation techniques. This approach has revealed the benefit of using software such as GoCAD as a data integration platform and FLAC as a process modelling tool. We have characterised the structural controls, ore distribution and thickness variations across the half-graben, which hosts the mineralisation. From this analysis we have been able to reconstruct the geometry and location of damage zones resulting from syn- to post-Isan Orogeny wrench style deformation, allowing also the distinction of early syn-sedimentary growth faults. 3D modelling has established overprinting relationships between temporally distinct hydrothermal events, and suggests a multistage evolution for this system. Fluid flow modelling using FLAC was aimed to test the control of permeability and deformation on subsurface fluid flow, i.e. a diagenetic or epigenetic model for fluid migration leading to mineralisation. However, this modelling shows that subsurface fluid flow through the mineralised shales was very unlikely to have occurred in preference to flow through faults and sandstones. Accordingly, both the spatial GoCAD and FLAC modelling suggests that a subsurface replacive origin for the mineralisation is less likely than a syngenetic model.

4.1.   Introduction

Plate tectonics has been recognised as a primary control on the nature and location of mineral deposits in the earth's crust. For example, Sawkins (1990) describes how different classes of metal deposits occur at specific locations of continental and oceanic margins. The relative abundance of metals and size of these occurrences depend on the tectonic context in which a mineral deposit forms as a direct function of the structural architecture, chemical composition of the crust, and type of mechanisms that allow the transfer of mineralising brines to produce economic grade mineralisation.

If we focus on shale-hosted Zn-Pb sulphide deposits (definition from Large 1980; Sangster 1983), we note that favourable present day sites for sulphide deposition are divergent plate boundary environments (e.g. median valley of the Red Sea; Degens and Ross 1969; Hackett and Bischoff 1973). This is represented by ore genetic models that invoke anomalous geothermal gradients as a key driving force for focussing metal bearing fluids along crustal discontinuities (e.g. SEDEX models), leading to ore deposition in rift dominated settings (Russell 1978; Goodfellow 1993). In contrast, not all Pb-Zn deposits occur in extensional setting, as several other varieties reportedly occur in compressional settings, during contraction (e.g., Garven 1985; Oliver 1986; Duane and de Wit, 1988; Bradley and Leach, 2003). Moreover, when giant accumulations of Zn-Pb are found in complexly deformed terrains (which record both extensional and compressional tectonic regimes), identifying the most favourable scenario for ore deposition becomes complicated. This issue is well known within the

Northern Australian Zinc Belt (Fig. 4.1), where many Zn-Pb occurrences (e.g. McArthur River, Mount Isa, George Fisher, Lady Loretta, Walford Creek and Century) are notable for their contentious genetic models.
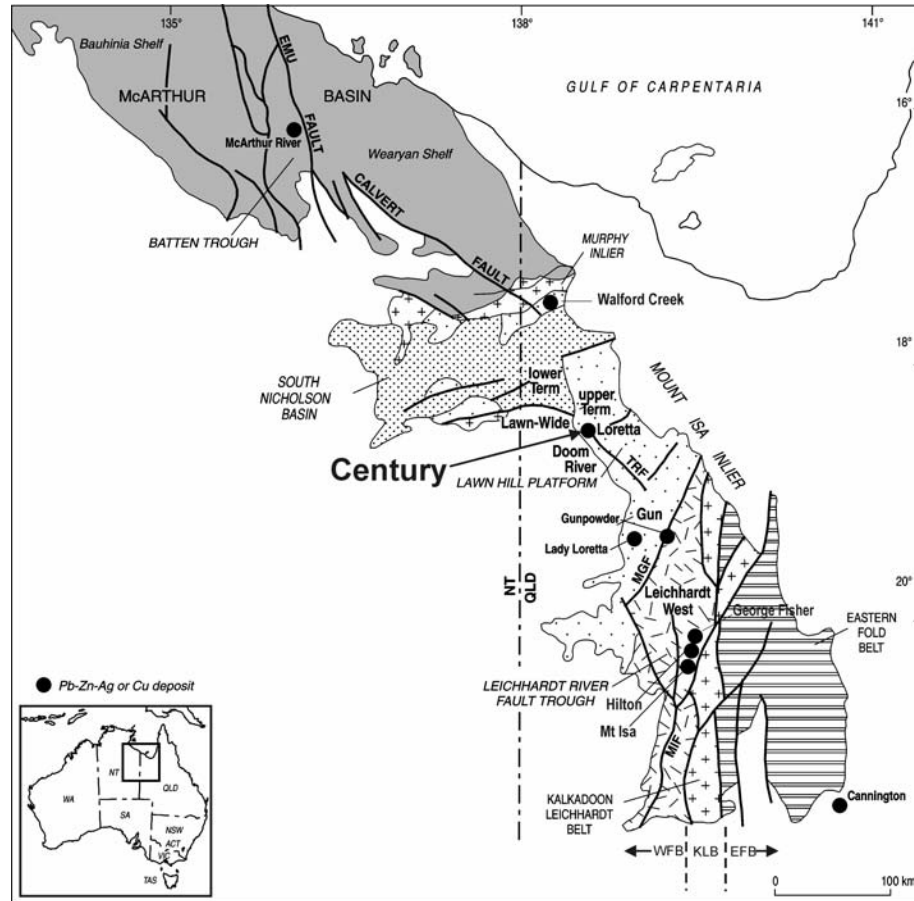

Fig. 4.1 Location map of the Century deposit and the major subdivisions of the Mount Isa Block and the Northern Australian Zinc Belt. The Mount Isa Block is subdivided into the main tectonic units of the Western Fold Belt (WFB), Kalkadoon Liechhardt Belt (KLB) and the Eastern Fold Belt (EFB). Major deposits (principally Zn-Pb-Ag) are shown and the Century deposit is highlighted in the Lawn Hill Platform (modified from Southgate et al., 2000).

A general method used to define the tectonic setting responsible for ore deposition, in the Mt Isa Block Zn-Pb deposits, has been to attempt to identify the relative timing of emplacement of massive sulphides with respect to the main stages of

Mesoproterozoic rifting, and to the Isan Orogeny (Fig. 4.2). Using paragenetic, structural, and geochemical constraints, previous authors have recently proposed different ore genetic models with syn-diagenetic timing for the George Fisher deposit (Chapman, 2004), syn-tectonic timing for the Mount Isa deposit (Davis, 2004), and syn-genetic timing for the McArthur River deposit (Ireland et al., 2003). It is clear that ore genetic controversies are still strong and may suggest:

a) That all these genetic models depict viable ore forming processes as Garven et al. (2001) proposes, and that a protracted hydrothermal evolution may have progressively accounted for the present metallogenic scenario within the Western Fold Belt (Sun et al., 1994), hence each deposit could have formed differently.

b) Only one of the above models (syn-sedimentary, syn-diagenetic, syn-tectonic) is valid for all these deposits.

c) Zn-Pb mineralisation is a result of a multi-stage hydrothermal evolution in which again all the models are viable scenarios, but all the deposits experienced a common hydrothermal history (i.e. remobilisation).

Some of the issues affecting these types of studies based on relative timing are:

1) Poor available constraints on the age of the Isan Orogeny (1585 - 1500 Ma) leading in some cases to possible overlap between depositional ages of sediments hosting the mineralisation (Page et al., 2000), and deformation ages (Connors and Lister, 1995; Connors and Page 1995). The Isan Orogeny itself has seen different deformational phases (e.g.

Bell, 1983, Bell and Hickey, 1996) and there is some possibility that the metamorphic peak and structural evolution may have been diachronous across the district (Table 4.1 also, compare Rubenach et al., 2001 and Giles and Nutman, 2003 with Oliver, 1995 and Bell and Hickey, 1996).

2) Presently accepted models fail to apply exclusively to specific tectonic scenarios, leading to confusion regarding the real ore genetic mechanism. For example, if we clearly identify the evidence for Mississippi Valley Type (MVT) mineralisation, in some cases it is not enough to sustain a contractional scenario for ore deposition. There are examples in the literature of rift-related Mississippi Valley Type Deposits; minor lead deposits found along the Red Sea coast of Egypt (Dadet et al., 1970; El Arif, 1984), and economic Pb-Zn MVT deposits that lie along the axis of the Benue Trough in Nigeria (Farrington 1952; Grant, 1971; Akande et al., 1988). After burial and subsequent metamorphism, it would be easy to interpret or misinterpret these mainly vein-hosted MVT ores as a syn-tectonic product.
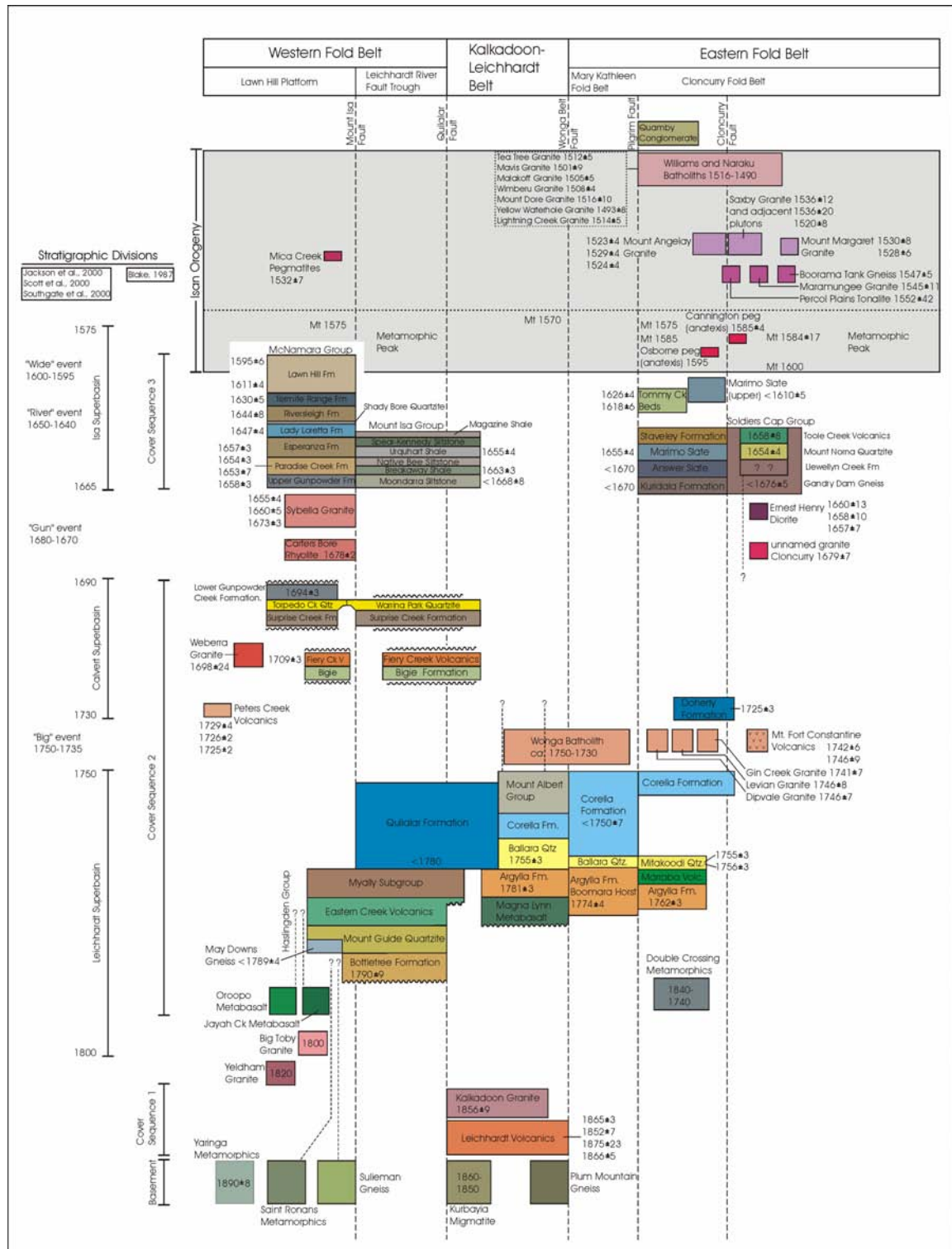
Fig. 4.2 (overleaf) Chronostratigraphy for the Mount Isa Block after Foster (2003). Modified from the compilations of Blake (1987), Blake and Stewart (1992), Page and Sun (1998), Page and Sweet (1998), and Page et al. (2000). Following Blake (1987), the stratigraphy is divided into 3 cover sequences, and divisions into the Leichhardt, Calvert and Isan supersequences. Delineation of the "Big", "Gun", "River" and "Wide" events are after Jackson et al. (2000), Scott et al. (2000), and Southgate et al. (2000). Age determinations for the stratigraphic units or intrusions are U-Pb zircon (mostly via SHRIMP) determinations, with exception of the pegmatites at Osborne (U-Pb titanite) and anatexis at Cannington (SHRIMP U-Pb monazite). Metamorphic ages (Mt) include U-Pb zircon and monazite (SHRIMP), and Sm-Nd garnet determinations. Detrital ages obtained from zircon constrain only the maximum possible age for the unit and are indicated by '<' at the front of the age.

Knowing these limitations we have attempted to use newly available computational tools to explore the problem of ore genesis from two new perspectives involving initially, 3D spatial/structural analysis (GoCAD), and subsequently, finite difference models of deformation and fluid flow (FLAC) that test one of the proposed ore genetic models for the Century Zn-Pb-Ag deposit.

Here, after a general introduction to the regional and local geology, we focus on the Century deposit considering the main features relevant to ore deposition. Revising and testing proposed ore genetic models, we re-interpret the genesis of Century based on the newly available data. However, the scope of this research also covers evaluation of the capacity of 3D modelling and FLAC modelling to answer ore genesis research questions.

4.2.   Tectonic evolution of the Mount Isa Block and

stratigraphic subdivisions

4.2.1.   The Mount Isa Block

The Mount Isa Block comprises three broad tectonic units; the Western Fold Belt (WFB), the Kalkadoon Leichhardt Belt (KLB), and the Eastern Fold Belt (EFB) (Fig. 4.1), which are predominantly north-south trending and separated by transcurrent fault zones (O'Dea et al. 1997; Blake and Stewart, 1992). Much of northern Australia underwent several periods of extension, leading to the development of intraplate sedimentary basins in which bimodal volcanic rocks and rift-sag sequences accumulated (Etheridge et al., 1987; O'Dea et al., 1997, Betts et al., 2003). The chronostratigraphic framework of the Mt Isa Block is outlined in Figure 4.2, and within the Mt Isa Block four major Proterozoic sequences are present (Blake, 1987). The oldest rocks, or basement, were first deformed and metamorphosed during the Barramundi Orogeny at approximately 1870 Ma (Etheridge et al., 1987). Following this orogeny, the Mount Isa terrain underwent a long and complex history of intermittent rifting and deposition, and several Palaeoproterozoic basins evolved between ca. 1800 and 1590 Ma (Carter et al., 1961; Smith, 1969; Plumb et al., 1980; Derrick, 1982; Blake, 1987; Page, 1988; Andrews, 1998; Page et al., 2000; Scott et al., 2000) in the North Australian Craton, which are best preserved and understood in the Mount Isa Block and McArthur Basin. Igneous and sedimentary rocks of this period were formed

or deposited during several superimposed intracontinental rifting episodes and associated post-rift subsidence, and designated Cover Sequences 1 to 3 (Blake, 1987) (see Fig. 4.2). Cover Sequence 1 (ca. 1870 – 1840 Ma) is restricted to a narrow central strip (Kalkadoon Leichhardt Belt) and consists predominantly of felsic meta-volcanic rocks. This belt acted as a 'high' and Cover Sequences 2 and 3 subsequently formed on the Eastern and Western sides (Eastern and Western Fold Belt Successions) during separate basin forming events.

Cover Sequence 2 was the result of a period of crustal extension from ca. 1790 – 1740 Ma, with early-syn-rift phase clastic sedimentary and bimodal volcanic rocks deposited in restricted fault controlled basins. These rocks were then overlain by clastic and carbonate sedimentation during a post-rift or sag phase, with termination of this cycle in the Eastern Fold Belt co-incident with the intrusion of the Wonga Batholith at around 1750 Ma (Stewart and Blake, 1992). Basement structures that developed during the deposition of Cover Sequence 2 appear to have had an influence on the depositional characteristics of Cover Sequence 3 (ca. 1670 -1595 Ma), which is best represented in the Western Fold Belt and unconformably overlies Cover Sequence 2. Cover Sequence 3 consists mainly of volcaniclastic rocks, conglomerates, sandstones, shales and carbonates, and is the host to Pb-Zn-Ag mineralisation in the Mount Isa Block. For a comparison between the Western, Kalkadoon-Leichhardt and Eastern Fold Belts, see Figure 4.2. Several attempts have been made to constrain the timing of the main deformational events in the Mount Isa Block during the Isan Orogeny, which vary substantially in relation to spatial aspects, isotopic dating and interpretation (e.g. cf. Page and Bell, 1986; Page and Sun, 1998; Bell and Hickey, 1996) (see Table 4.1). More

recently Giles and Nutman (2002) challenged the common perception of orogeny in the Mt Isa Block in which 'peak metamorphism', and the deformation events associated with it, can be correlated across the entire Mount Isa terrane.

Table 4.1. Correlation of deformational history in three locations of the Mount Isa Block, including a summary of age dates from several locations.

Deformation Event	Eastern Fold Belt Age	Western Fold Belt Age	Selwyn Region Adshead-Bell (1998)	Selwyn Region Jaques et al. (1982)	Selwyn Region Beardsmore (1988)
D_1 N/S Compression		D_1 - 1610 ± 13 Ma (Page and Bell, 1986)	D_1		D_1
D_2 E/W Compression	U/Pb 1584 ± 17 Ma (Page and Sun, 1998) Ar/Ar 1590 Ma (Perkins and Wyborn, 1998) 1580 -1600 Ma (Giles and Nutman, 2002)	D_2 - 1544 ± 12 Ma (Page and Bell, 1986) 1580 ± 5 Ma (Hand and Rubatto, 2002)	D_2	D_1	D_2
D_3 E/W Compression		$D_{2.5}$ (Bell and Hickey, 1986)	D_3		
D_4 E/W Compression	U/Pb $1493 – 1508$ Ma (Page and Sun, 1998)	D_3 - 1510 ± 13 Ma (Page and Bell, 1986)	D_4	D_2	D_3
D_5 E/W Compression			D_5		
D_6 E/W Compression		D_4 (Bell and Hickey, 1986)	D_6		D_4

4.2.2. The Western Fold Belt

In the Western Fold Belt three superbasins have been identified and delineated; the Leichhardt Superbasin (ca. 1800 -1740 Ma), Calvert Superbasin (ca. 1730 – 1690 Ma) and Isa Superbasin (ca. 1665 – 1575 Ma) (Fig. 4.3). Preceding the development of

the Isa Superbasin, a complex history of extensional basin development, sedimentation and volcanism resulted in two superimposed and unconformity bounded basins; the Leichhardt Superbasin and the Calvert Superbasin. The Leichhardt Superbasin, which was controlled by half-graben bounding faults (O'Dea et al., 1997), is essentially comprised of shallow marine and fluvial sediments and bimodal igneous rocks and formed during the Leichhardt Rift Event (Betts and Lister, 2002) (Fig. 4.3). Basin inversion then followed, with localised shortening evident in the Leichhardt Superbasin (Betts et al., 1999). Following basin inversion extension was accompanied by shallow marine and fluvial sedimentation and bimodal volcanism in developing half-grabens (Betts et al., 1998; 1999; Southgate et al., 2000) in association with the development of the Calvert Superbasin (Jackson et al., 2000) and the Mount Isa Rift Event (O'Dea et al., 1997).

Reactivation of N-S rift bounding faults and E-W cross-rift faults during the Mount Isa Rift Event to some extent controlled the architecture of the Calvert Superbasin and subsequent sedimentation. Half-graben bounding faults were active in the Lawn Hill Platform and transverse faults, such as the Termite Range Fault, were considered active during deposition of the Isa Superbasin (Scott et al., 2000). The Isa Superbasin has been interpreted as the result of a sag phase or thermal subsidence (Betts et al., 1998). This subsidence appears to have been more extensive to the west/northwest of the Leichhardt River Fault Trough (Fig. 4.1), which resulted in extensive deposition of carbonaceous shale, sandstone and siltstone and formed the McNamara Group (ca. 1660 – 1595 Ma) which is the host to the major shale-hosted massive sulphide Pb-Zn- Ag deposits of the region (Fig. 4.4). Most deposit Pb-Pb or U-

Pb ages correspond well with their host successions, Century being the main apparent exception which is dated at around 1575 ± 6 Ma (Carr, 1996), 20 Ma younger than the 1595 ± 6 Ma host sediments. However, the Pb isotopic ratios could have been potentially influenced by later more radiogenic fluids. Moreover, the 1595 ± 6 Ma age for the H4s re-sedimented tuff-beds are maximum ages that do not necessarily coincide with the sedimentation age, and could be younger, overlapping with mineralisation timing in analogy to e.g. Mount Isa, McArthur River (HYC) and Broken Hill.

This extensional history and overall basin development was interrupted by compression, basin inversion and regional wrenching during the Isan Orogeny ca. 1585-1500 Ma (O'Dea et al., 1997, Betts et al., 1999; Betts et al., 2006). The subdivisions of the Mt Isa Block display contrasting responses to deformation in the region, with associated strain less intense in the Western Fold belt than that of the Eastern Fold Belt due to strain accommodation by underlying basin fault architecture (Betts, 2001). In the Eastern Fold Belt thin-skinned tectonics dominate with shallow dipping faults, whereas in the Western Fold Belt, brittle deformation affected much of the upper crust. The Kalkadoon-Leichhardt Belt consists of older, exposed basement rocks which accommodated the deformation by working as a buttress during periods of crustal shortening (Drummond et al., 1998).
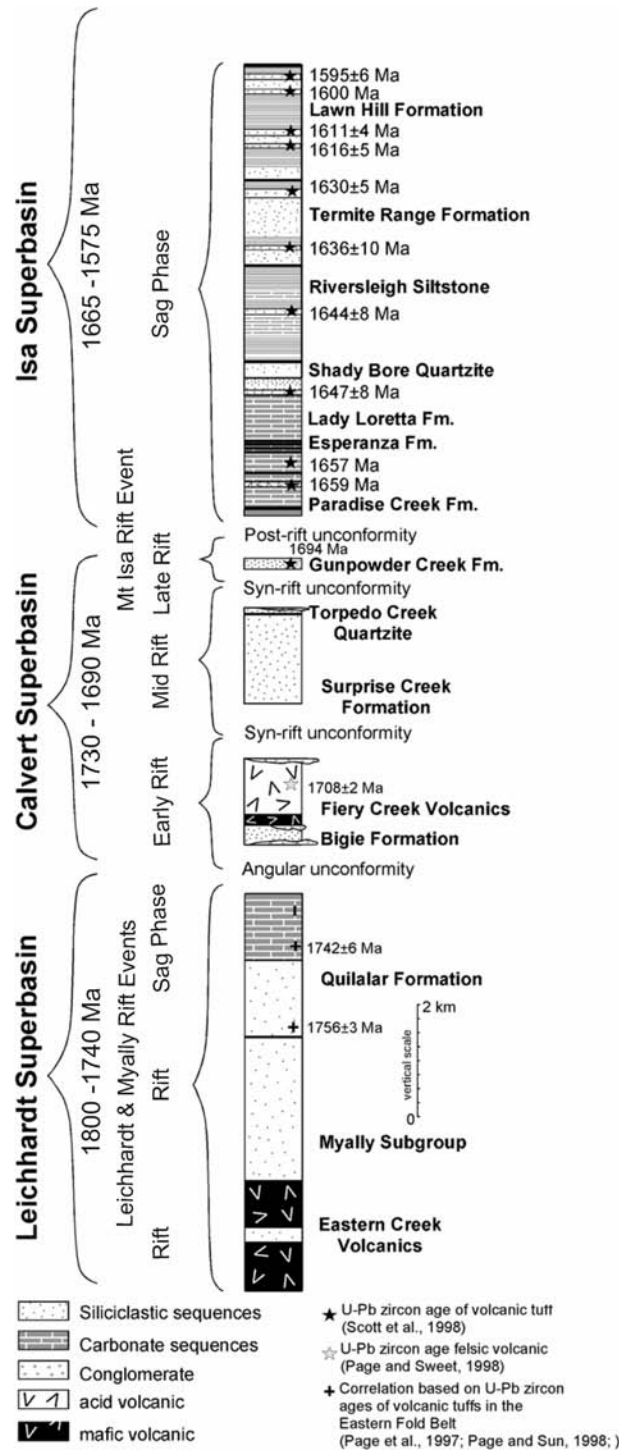
Fig. 4.3 Simplified lithostratigraphic column of the Western Fold Belt displaying the three Superbasins and associated rifting sequences. Geochronological data after Scott et al. (1998), Page and Sun (1998), Page and Sweet (1998) and Page et al. (2000), (modified from Betts et al., 2003).
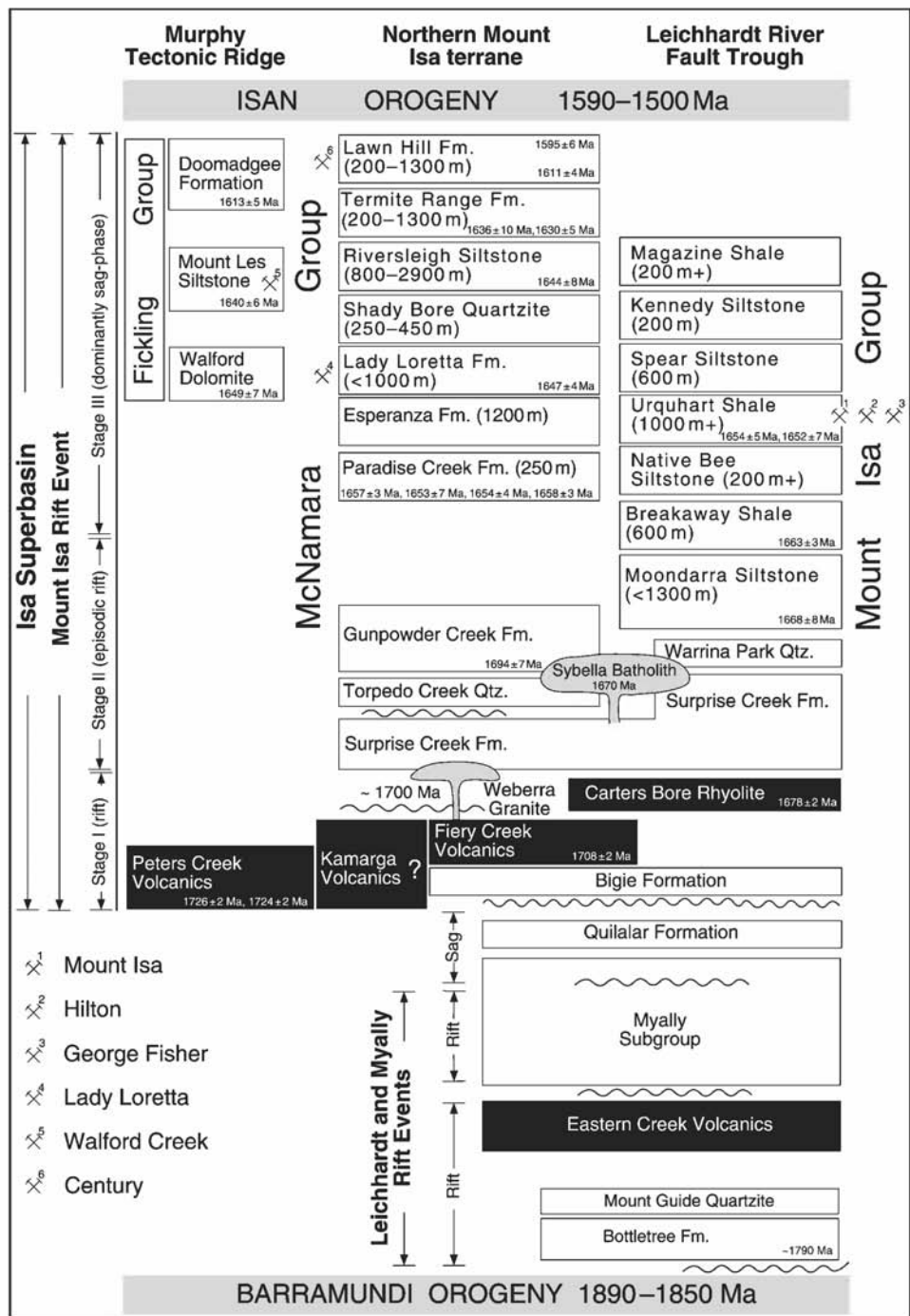
Fig. 4.4 Stratigraphic correlations in the Western Fold Belt displaying the major ore deposits and the age of stratigraphic horizons within the McNamara Group, (after Betts and Lister, 2002).

4.2.3. Stratigraphy of the Lawn Hill Formation

The Lawn Hill Platform (Plumb and Derrick, 1975) represents the northern part of the Western Fold Belt (Fig. 4.1). Here, Zn-Pb mineralisation (e.g. Century zinc deposit) occurs preferentially in a number of stratigraphic layers hosted in the McNamara Group (Fig. 4.5).
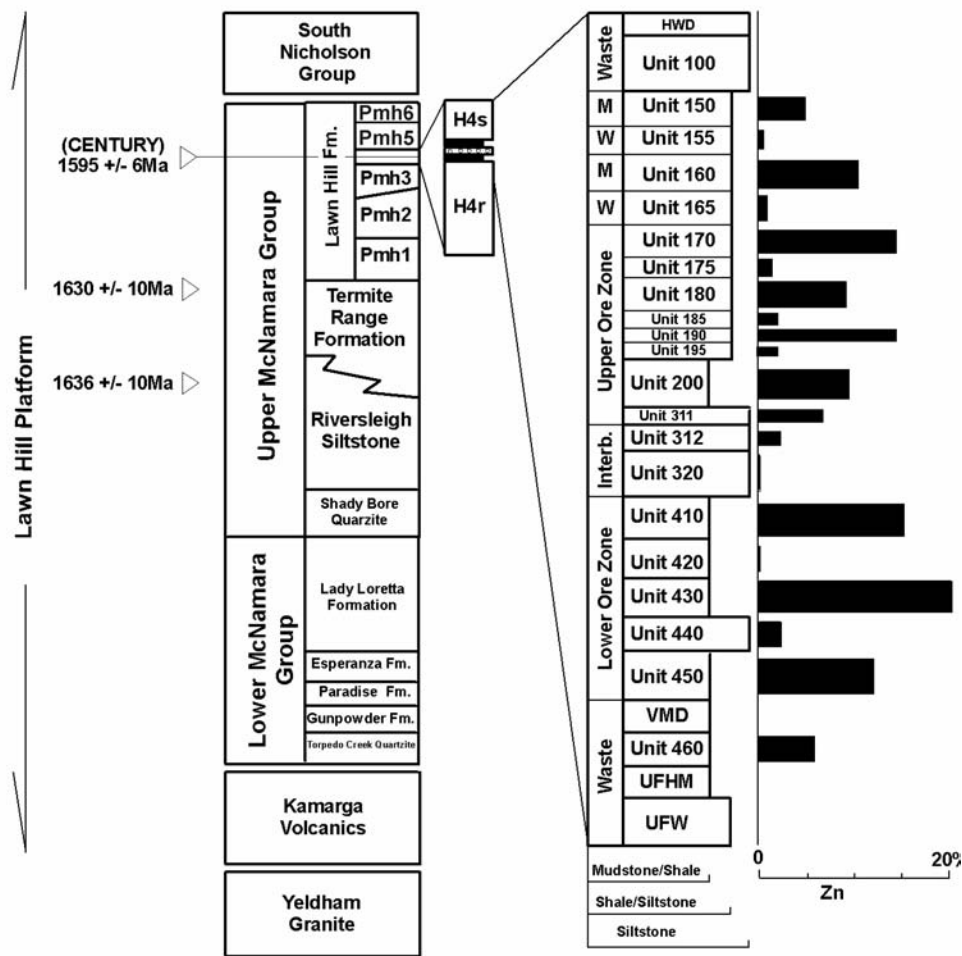

Fig. 4.5 Stratigraphy of the Lawn Hill Platform indicating the relative location of the Century Deposit and stratigraphic ages. On the right is a detailed stratigraphy of Member Pmh4 with the Century Ore Zone linked to grade distribution of %Zn.

Previous interpretations of O'Dea et al. (1997) and O'Dea and Lister (1995) view this thick package of sediments as being deposited during alternative phases of rift and sag episodes, with no significant tectonic activity (Betts, et al., 1998). Scott et al., (1998) and Krassay (2000b) reinterpreted the seismic stratigraphy of this package of sediments, suggesting that several tectonic events occurred during and after sedimentation. Syn-sedimentary deformation is documented by the identification of syn-sedimentary growth faults across the Elisabeth Creek zone. The most obvious structural feature in the region is the northwest striking Termite Range Fault (Andrews, 1998; Betts et al., 1998; Broadbent, 1999) which has been considered the major fluid pathway for mineralisation (Broadbent et al., 1998). The Termite Range Fault (TRF) has been described as a long-lived transverse fault (Betts, et al., 1999; Ord et al., 2002) and was most likely active for > 140 million years. The TRF has had a major influence in the deposition of sediments throughout the upper McNamara Group and has localised sedimentary depocentres (Andrews, 1998). Lateral variations in sedimentation can be found in and around the Century deposit suggesting local thickening, which Broadbent et al. (1998) describes as a result of parasitic faults emanating from the TRF. However, other east-northeast and northeast striking, steep, reactivated faults represent an important characteristic of this region, and were probably also important in transferring brines and controlling deposit locations across the Lawn Hill Mineral Field (see below).

The McNamara Group rocks in the Lawn Hill Platform form the youngest cover successions of the Mount Isa Block, correlative with the Fickling Group (Sweet et al., 1981; Blake, 1987; Blake and Stewart, 1992; Andrews, 1998; Krassay, 2000a) (see Fig. 4.4). The upper McNamara Group comprises up to 7500 m of deep marine, paralic and

terrestrial, siliciclastic-dominated facies of the Shady Bore Quartzite, Riversleigh Siltstone, Termite Range Formation, and Lawn Hill Formation. The Century orebody and surrounding vein-hosted mineralisation is stratigraphically constrained within the upper part of the McNamara Group in the Termite Range Formation and Lawn Hill Formation. This was subdivided by Sweet and Hutton (1982) into six members, Pmh1-Pmh6 (Fig. 4.5). Andrews (1998) distinguished two additional members: H1s within Pmh1 and H4s (host to Century Zn-Pb-Ag mineralisation) at the top of member Pmh4 (Fig. 4.5). Members Pmh1, Pmh2, Pmh4 and Pmh6 are dominantly fine grained and carbonaceous and represent a low energy, deep subaqueous environment. Pmh3 is a sandy interval and represents a shallower, higher energy marine setting. Member Pmh5 comprises thick lithic and feldspathic sandstone interpreted either as high-energy marine shelf deposits (Sweet and Hutton 1982) or sandy turbidites (Andrews 1998). More recently, after the accomplishment of the North Australian Basin Resource Evaluation (NABRE) project, the lithostratigraphy has been reorganised in light of new concepts of sequence stratigraphy (refer to Southgate et al., 2000; Neumann et al., 2006). Outcomes of the NABRE project resulted in an updated stratigraphy that is based on erosional and maximum flooding surface boundaries, new geochronology results (Page et al., 2000), and also palaeomagnetic data sets to constrain the depositional conditions (Idnurm, 2000; Southgate et al., 2000).

In sequence-stratigraphic terms the Lawn Hill Formation comprises the upper part of the Term Supersequence and the Lawn, Wide and Doom Supersequences (Krassay et al., 2000b) (see Fig. 4.6). The Century zinc deposit is hosted in the Wide supersequence (Wide 1), representing a third order maximum flooding surface,

suggesting low energy conditions. As relative sea level reached this maximum flooding surface, basins became starved of sediment deposition, resulting in a condensed section, which may have favoured the concentration of sulphides, particularly in shale units (Ruffell, et al., 1998).
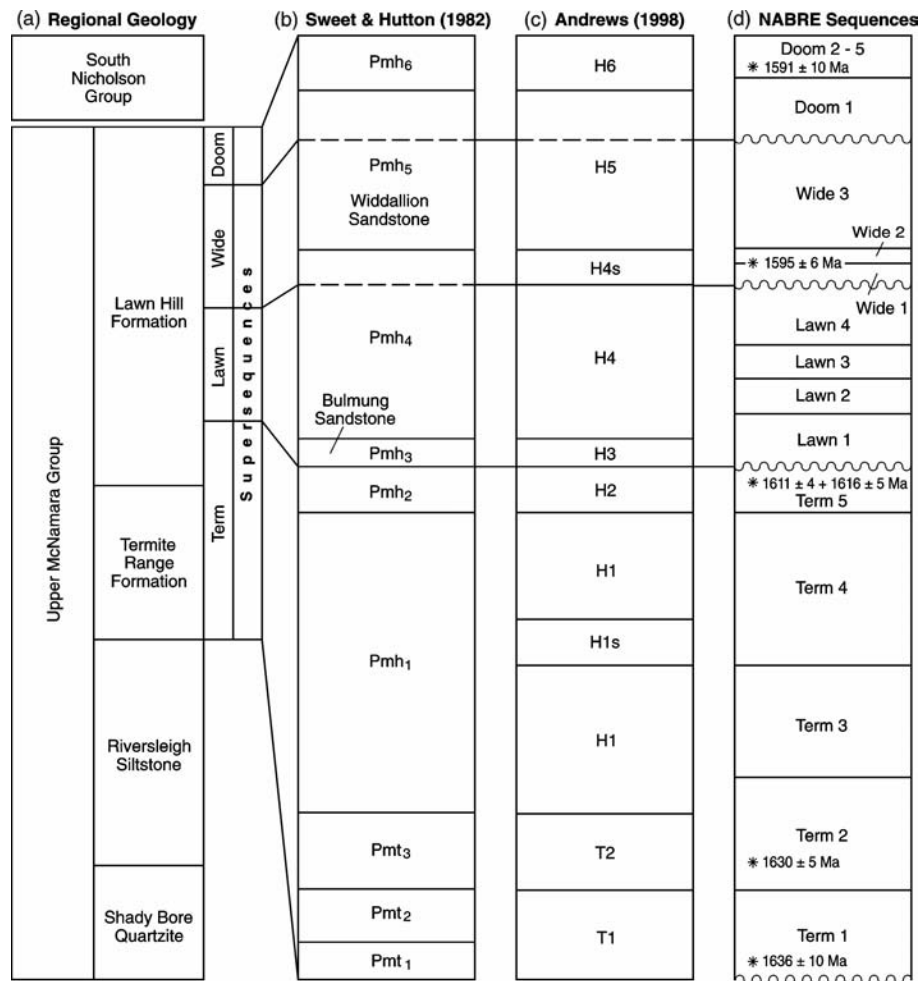

Fig. 4.6 Stratigraphic columns comparing the various classification schemes for rocks of the upper McNamara Group. (a) Regional geology for entire McNamara Group. (b) Upper McNamara Group formally defined lithostratigraphic units after Sweet and Hutton (1982). (c) Upper McNamara Group informal lithostratigraphic units by Andrews (1998). (d) North Australian Basin Resource Evaluation (NABRE) sequence-stratigraphic terminology and SHRIMP depositional zircon ages from the central Lawn Hill Platform. After Krassay et al. (2000a, b).

The Lawn Hill Formation contains tuffs and reworked tuffs at a number of stratigraphic levels. Page and Sweet (1998) dated a population of zircons (1595 ± 6 Ma) in the mineralised member Pmh4 (from Century drill core). Page et al., (2000) also presents consistent results from four new samples, two from member Pmh2 (Lawn Supersequence, 1616 ± 5 Ma; 1611 ± 4 Ma) one from member Pmh4 (Lawn Supersequence, 1595 ± 6 Ma) and one most likely derived from member Pmh6 (Doom Supersequence, 1591 ± 10). The ages derived from Pmh2 (1616 ± 5 Ma and 1611 ± 4 Ma) are stratigraphically in accordance with the age of 1595 ± 6 Ma for Pmh4. Well established geochronological constraints, coupled with sedimentary evidence presented by Krassay et al., (2000a), argue strongly for a tectonic control of the major (2nd-order) supersequences, and most 3rd-order accommodation cycles (sequences) across all of the Isa Superbasin. Evidence of a tectonic influence includes facies changes and thickness trends related directly to active faults, partitioning of depocentres by these faults, abrupt provenance switching, tilting and erosion of older sedimentary sequences. Furthermore, Krassay et al., (2000a) suggests that the Isan Orogeny may have commenced during deposition of Doom 4 and Doom 5. These final considerations suggest that the D1 phase of the Isan Orogeny probably post-dated the depositional age of sediments hosting the Century mineralisation.

4.3.   Century deposit

The Century deposit is one of the largest Zn-Pb-Ag accumulations in the world with a mineral resource of 138 Mt at 8.23% Zn, 1.16% Pb, and 29 g/t Ag (Clifford and

Kelso, 2003). This stratiform mineralisation has not been as extensively studied as other Zn-Pb metal occurrences in the Isa and McArthur Superbasins e.g., Mount Isa, McArthur River (HYC), Lady Loretta etc., as it is one of the more recent discoveries (1990 CRAE exploration Ltd.).

4.3.1. Sulphide textures

The main stratiform mineralised units are a finely laminated shale unit consisting of essentially fine grained sphalerite and siderite with minor galena and pyrite. The presence of hydrocarbons or pyrobitumen with porous sphalerite has been discussed in detail by Broadbent (1999). However, the non-porous sphalerite has no clear relationship to pyrobitumen; it also has the highest grade and volume within the mineralised sequence. The subdivision Pmh5, which is comprised of a thick (~150 m) cemented chlorite rich sandstone lies directly above the 'ore zone'. Broadbent (1999) and Ord et al., (2002) have interpreted this unit as a potential seal in the system due to its characteristics and early cementation (Andrews, 1998). Discordant mineralisation (at meso-scales) is relatively minor, and comprises veins and irregular patches, typically galena-dominant (Broadbent et al., 1998). Vein-style mineralisation which is completely discordant to bedding is common in an area of about a 30 km radius around Century (e.g. Silver King, Waltho and Andrews, 1993).

4.3.2. Ore zone stratigraphy

The mine stratigraphy is contained in the subdivision Pmh4, which is comprised of over 500 m of interbedded siltstone and shale units with minor mudstone, is summarised in Figure 4.5. Logging of ore zone units has suffered from inconsistent unit definitions in the past. With the completion of re-logging in the Solid Geology project the ore zone units are now much more consistently constrained (Fig. 4.7).

The upper ore zone generally consists of interbedded siltstone and shale bands (Fig. 4.7), and varies from very well laminated to stylolitic layers, with evidence of layer parallel shearing in several units. Unit 200 (3-5 m) is the first major ore unit but has quite a different appearance in Stages 1 and 2 (the southern part of the mine) to the majority of the north block. In Stages 1 and 2 this unit was commonly a massive mudstone interval which was frequently brecciated and deformed by bedding parallel shear, coincident with high lead grades. In the north block the unit occasionally suffers bedding parallel shear within laminated shale (similar to Unit 160), mudstone intervals are rarer. Unit 310 is a transitional unit from the shales of Unit 200 to the siltstones of Unit 320. As the upper part of the unit can contain some very high-grade mineralisation it has been split into Units 311 and 312 on the basis of assay information (Unit 311 is > 6.5% Zn).

THIS TABLE HAS BEEN REMOVED DUE TO
COPYRIGHT RESTRICTIONS

Fig. 4.7 Stratigraphic summary and description of the Century Deposit (courtesy of Century mine & I. Kelso)

The relative thickness of these units is variable and either can comprise the entire interval. If there is no assay information or the unit is affected by hematite alteration it is logged as Unit 310. Unit 311 is the lowest unit in the Upper Zone ore and Unit 312 is the first unit of Internal Waste. Interburden within the ore zone relates to Unit 320 (2.5-3.5 m) and was called the Cappuccino zone by CRA due to the sideritic buff coloured stylolitic siltstones, which comprise the entire interval and the majority of the Internal Waste. The lower ore zone generally consists of high-grade well-laminated black shale with interbedded mudstone.

4.4.   Introduction to the 3D structural modelling

The primary objective of almost every geological characterisation is concerned with predicting the spatial variation of one or more geological variables (Houlding, 1994). A conventional approach that is commonly used to define a geological entity is a 2D representation of the geology using a map or a cross-section, as our ability to deal with geometrical problems in 3D is limited and it is difficult to represent it visually. However, since the advent of computerised methods, defined as CAD (computer aided design), most of these difficulties have been overcome, enhancing our understanding and providing new ways of dealing with complex geometrical problems in 3D space. In computer aided design, a geological scenario requires a mathematical description of the components. This process happens when we adopt algorithms that use discretization and qualification of irregular geological space into irregular volumes, with similar

distinguishing characteristics. Some of the most common characters used to define geological space are lithological subdivisions or physical properties such as density, permeability and mineralisation content, amongst others.

Several types of investigative sources are available and are commonly used to gather the information necessary to construct a generic model, which comprises a set of well constrained geological spaces. The implemented data, when we consider the representation of a mineral deposit, are generally of two types a) a direct sampling of a discrete and representative quantity of rock, soil or unconsolidated sediment; or b) an indirect quantification of a property of the geological space using i.e. topographical, geochemical, or geophysical investigations. This information is made up of a range of observations that must be weighted. For example, we might have data that is collected in outcrops with 99% confidence on its location and geological characteristics, or a geophysical survey that can be regarded as fuzzy in terms of location and geological characterisation. Thus, there is a need to quantify the quality of the information available considering its source, before we integrate it within a generic 3D model. Creating geologically relevant 3D models from low relief, poorly exposed and geologically complex regions is a daunting if not impossible task (de Kemp, 2000). As a consequence, it is also important to have a clear understanding of the spatial density distribution of data used during the interpretative construction of the geology.

Once the representative geometries are defined, the evaluation of the results of a geological characterisation typically involves spatial analysis of the variation of one or more variables. This can be done using modern visualisation tools that allow not only a rapid correlation analysis, but also an interactive query of the database that creates the

3D model. This consents to quantifying the information displayed, facilitating its understanding.

4.4.1.   GoCAD a 3D geologically optimised CAD package

GoCAD is a software that allows the reconstruction of geological objects in 3D (see Chapter 2) and was used to construct the model of the Century deposit. An important advantage of this software is that it consents the definition of several types of constraints (Chapter 2), some of them may be imposed to respect the data inserted within the model, others can be used to fit the structural interpretation when the data are incomplete. Constraints are useful for example when modelling stratigraphic layers and faults. The final 3D model represents therefore a combination of data interpolation, and geological interpretation imposed by the user during the modelling process.

4.4.2.   Initial steps to construct a 3D model

The basic requirements and procedures adopted to construct the 3D model of the Century Zn-Pb-Ag deposit can be summarised as a sequence of clearly defined steps:

- *Management, Correlation and Integration* of the various information sources available from site investigation. The most important, and potentially most time consuming, aspect of this step is spatial correlation of the available data sources.

- *Review and Analysis* of the information sources in terms of their quality, sufficiency, scale and spatial variability. This provides an initial appreciation of the complexity and magnitude of the conditions we have to deal with. It also allows us to identify the geological characters that influence the spatial variation of the variables of interest.

- *Interpretation* of geological stratigraphy, structure and other relevant factors, based largely on observation of characteristics. The result is a discretization of the subsurface continuum by controlling geological characteristics. The operative term here is *interpretation,* because we are commonly forced to apply our geological intuition and experience to compensate for limited primary data.

- *Prediction* of the spatial variation of relevant variables based on sample information, geological interpretation and appropriate prediction techniques. The operative term in this case is *prediction*, the true conditions are seldom determinate from limited information and our predictions are always subject to some degree of uncertainty.

- *Spatial Analysis* of the interpreted and predicted information, generally in terms of volumetrics and visualisation procedures, and/or transfer of the characterisation results to the relevant end process, such as mine planning or fluid flow modelling.

4.4.3.   Data acquired to construct the 3D model

To construct the 3D model of Century and the Lawn Hill mine lease area we have initially developed a mine scale model that uses most of the data collected during exploration and resource evaluation carried out initially by Rio Tinto, Pasminco, and subsequently by Zinifex Pty Ltd, and also a range of data gathered during recent exploitation activities, which involved the design and development of several open-cut stages. In a second, more advanced phase of this project, we have integrated the deposit model with selected data at regional scale. The main sources of data were: (a) the Pasminco Century mine database; (b) Solid Geology reports; and (c) aerial photography.

4.4.4.   3D model components

The Century model in its final stage includes a highly detailed 3D reconstruction of the faults at the deposit and regional scale, a set of horizons representing the topology of some of the highly mineralised intervals, and a Digital Terrain Model (DTM) representing a 3D reconstruction of the mine lease. Interesting results were obtained when comparing the data at different scales, and projecting some of the drilling database information over the mineralised Unit 200 (see Fig. 4.7) with the intent of visually evaluating the relationship between fault distribution versus thickness and grade variation across the Century deposit. Unit 200 was utilised as it was the reference based unit for mine geologists at Century, being the easiest to log.

4.4.5. 3D Modelling results

As mentioned in the initial introduction of this chapter we have attempted to use the 3D model to gain insights into ore genetic processes. After this initial consideration we have defined three research questions as follows:

(1) What was the link between the fault architecture and the mineralisation within the Lawn Hill Mineral Field?

(2) What were the faults that may have contributed to ore transport and deposition other than the Termite Range Fault?

(3) Which structures were the primary growth faults within the Century system, and did they play an important role for mineralisation?

To answer these questions we have tried to identify if regional scale faults mapped in 3D using the DTM (Fig. 4.8a) (in combination with aerial photography), intersect the mineralisation at depth. We also used the model to define what the important faults for mineralisation were, and we attempted to evaluate the relative timing of faulting events.

The rapid visualisation of all the structural data using GoCAD, reveals continuity between NE trending regional scale structures and faults within the Century deposit (Fig. 4.8a, b). We recognise that the regional Silver King Fault (SKF) most likely intersects Century. This link is supported further by a range of data that includes thickness variations and grade distributions at the Century scale (see below), and the topology of the Hangingwall Sandstone (see Fig. 4.7) surface in the hangingwall of the ore zones. Within the deposit we also recognise that the evolved geometry of the

Termite Range Fault (TRF) is surely the result of significant reactivation. Moreover, it is important to remark that NE striking faults were coevally active with the Termite Range Fault from early stages of sedimentary deposition. Evidence of NE structures, intersecting older sediments of the Termite Range Formation, indicates a similar history of reactivation. However, several faults mapped in the pit area are relatively young parasitic branches (e.g. Gecko and Prosperity system faults) of TRF, and most likely developed during the later phase of wrench style deformation (Fig. 4.9). These faults seem to have only partially influenced the present distribution of ore. Superimposed on these events is a final extensional stage that has contributed to the present half graben structures and has subdivided the Century deposit in three independent fault blocks separated by E-W striking structures (e.g. Pandora's Fault). The NE structures can be interpreted as reactivated as some of them displace the E-W faults. The trace of the SKF corresponds well to a significant zone of thickness variations observed within the deposit, (Fig. 4.10a, b) and most likely represents a reactivated growth fault; however some of the thickening could be due to later localised thrusting, especially within the shale 200 interval. The topology of Unit 200 is not influenced by significant deformation along the SKF, possibly supporting the growth fault model. However, this might be due to a different response of the shales (less competent units) to subsequent deformation. In addition, the shales show some evidence of parallel bedding shear.
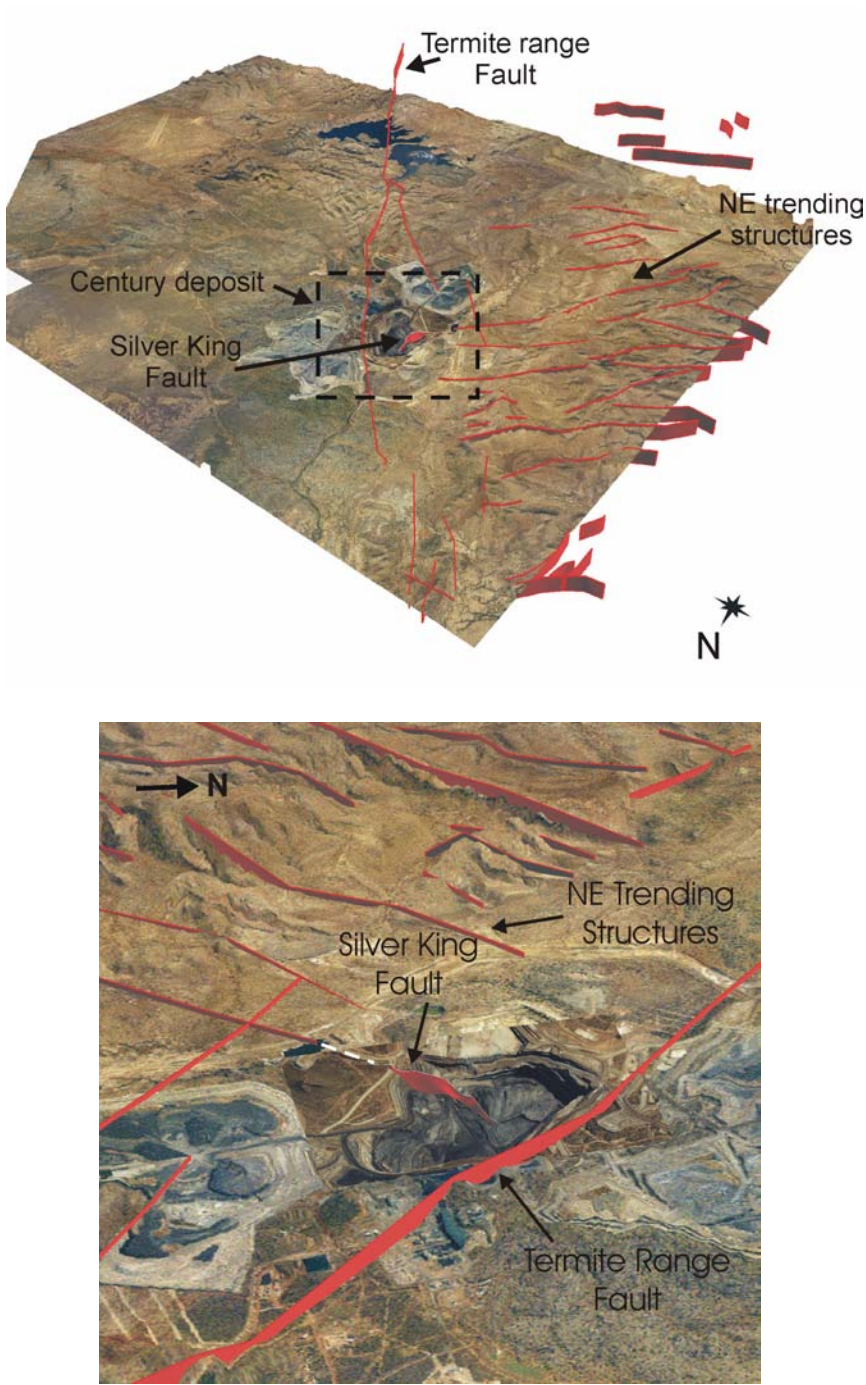
Fig. 4.8 Digital Terrain Model (DTM) of the Century deposit and surrounding region. (a) Century deposit and NE trending structures. (b) Digital terrain Model (DTM) of the Termite Range fault intersecting the Century deposit, and highlighting the potential link between NE trending regional structures and the Silver King Fault.
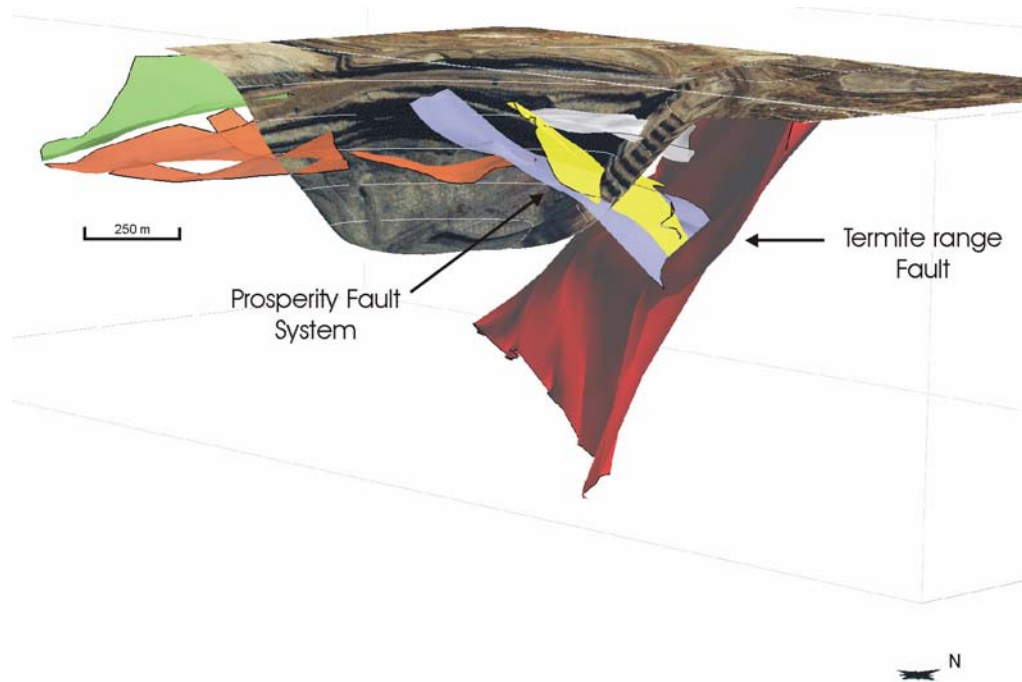
Fig. 4.9 Digital Terrain Model (DTM) integrated with 3D structural data, highlighting the Termite Range Fault and the parasitic Prosperity Fault system.

Grade distributions of both Zn and Pb correlate well with NE trending structures and Pb distribution in Unit 200 displays higher grades closer to the TRF (Fig. 4.11a, b) also associated with NE trends. The distribution of Zn in Unit 200 displays isolines with similar NE trends; and the high grade Zn zone overall is distal relative to the TRF (Fig. 4.12a, b). The isopach map of Unit 200 indicates that major sedimentary thickening occurs in the south eastern corner of the deposit and also within channelled domains in the northern block. In both cases the thickening seems to be associated with NE trending structures if we consider the distribution of isolines. These NE trends of thickness are parallel to trends observed in the Pb and Zn grades.
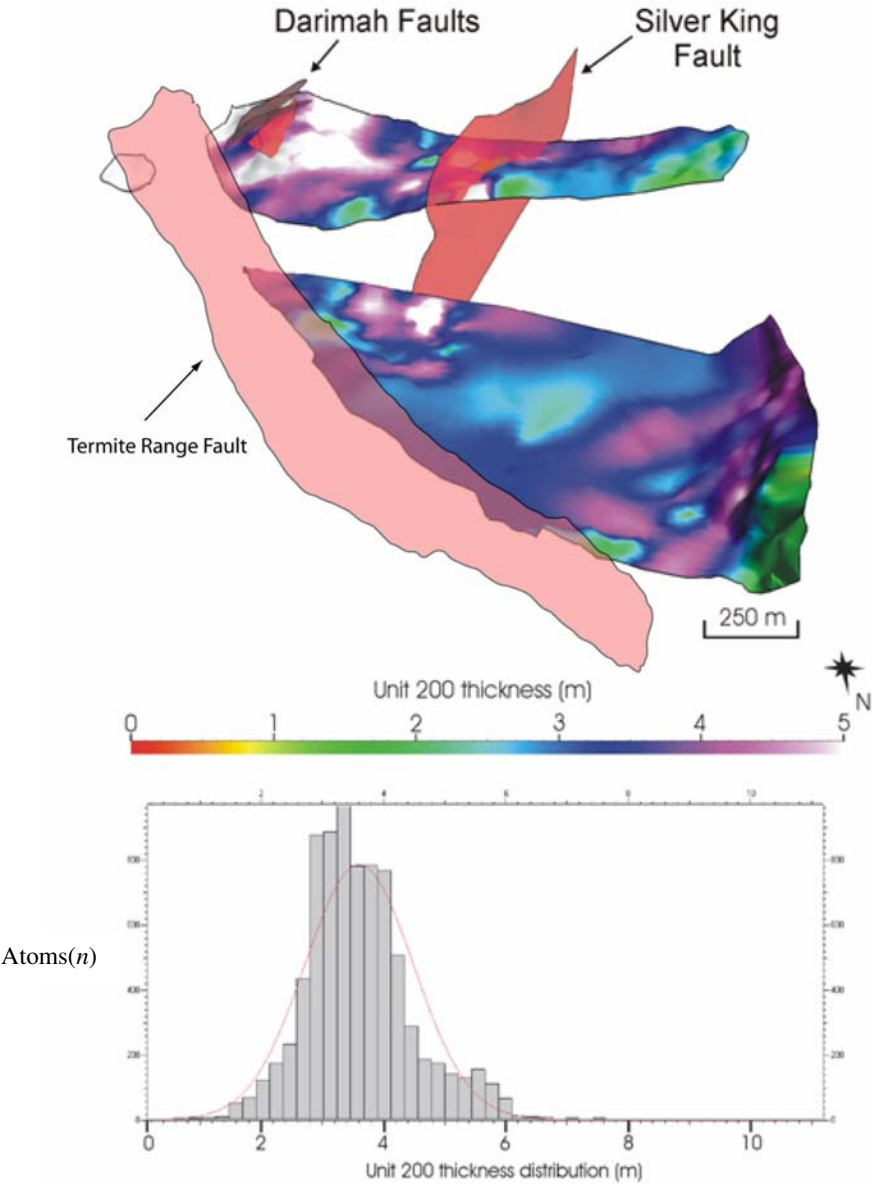
Fig. 4.10a. 3D representation of the thickness variation in Unit 200 of the Century deposit looking south. Note the correlation of thickness increase with NE trending faults. Below: Histogram displaying the thickness distribution of Unit 200.
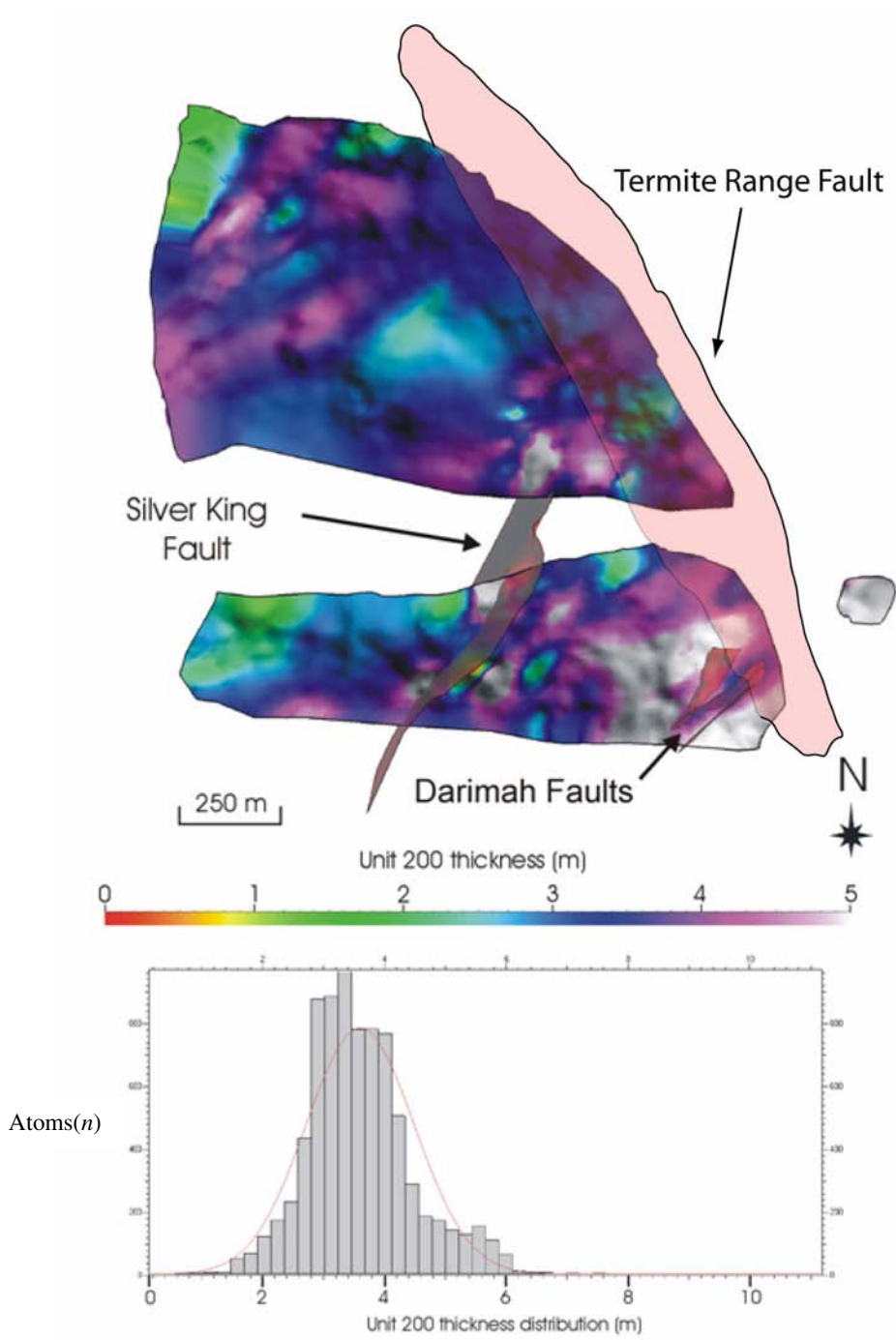
Fig. 4.10b 3D representation of the thickness variation in Unit 200 of the Century deposit looking north. Note the correlation of thickness increase with NE trending faults. Below: Histogram displaying the thickness distribution of Unit 200.

In summary the main conclusions made in relation to this study are:

- The 3D model shows that not only the TRF was active, and played a significant role in ore deposition processes, but other active faults in the system display correlations with thickness and mineralisation. The intersection of NW and NE structures could have been particularly important in focussing fluids

- The geometry of the TRF is the result of significant reactivation; however, several faults that have similar strike to the TRF, but dip towards NE, were interpreted to be relatively young parasitic branches of the TRF and were developed more likely during wrench style deformation occurring post-basin inversion, during the later stages of the Isan Orogeny.

- Bedding parallel shear is a characteristic of the shale's response to the brittle deformation. Much of this deformation may be younger than the main movement on the TRF as it does not seem to have a major influence on the mineralisation. Some localised redistribution of galena, that we interpret as a product of internal remobilisation of laminated ore, occurs exclusively in bands included within specific mine stratigraphic units (e.g. Unit 180) with higher Pb weight % contents.

- Metal distributions for Zn and Pb within Unit 200, which is one of the better constrained units in the upper ore zone, have pointed out the importance of NE trending structures as active faults that controlled ore emplacement.

4.5.   Century ore genesis

Two ore genesis models have been proposed for Century, based largely on paragenetic and geochemical work. The first model proposes an early-diagenetic timing of mineralisation (Waltho and Andrews, 1993). Following this work, Broadbent et al. (1998) has reinterpreted some of the textural arguments proposed as evidence of syngenesis to early-diagenesis and using new available lead, sulphur and carbon-oxygen data constrained using his detailed paragenesis, argues that a late-diagenetic to syn-tectonic timing for the mineralisation was more likely at Century. The main geological constraints and evidence for the Century late-diagenetic ore genesis following Broadbent et al. (1998) were:

(1) Overall zoning of ore and gangue mineral assemblages.

(2) The lack of any complex silicate- or barite-bearing assemblage indicative of exhalite facies anywhere within the (preserved) deposit stratigraphy.

(3) The consistent stratigraphic thickness of shale horizons which host ore, regardless of total sulphide content or grade of mineralisation.

(4) The transgressive nature of mineralisation at the overall scale of the deposit.

(5) The intimate associations of siderite, sulphides, and pyrobitumen at microscopic scale.

(6) Progressive timing relationships of silica mobility, siderite deposition, and sulphide deposition relative to compaction and dissolution fabrics of the host sequence.
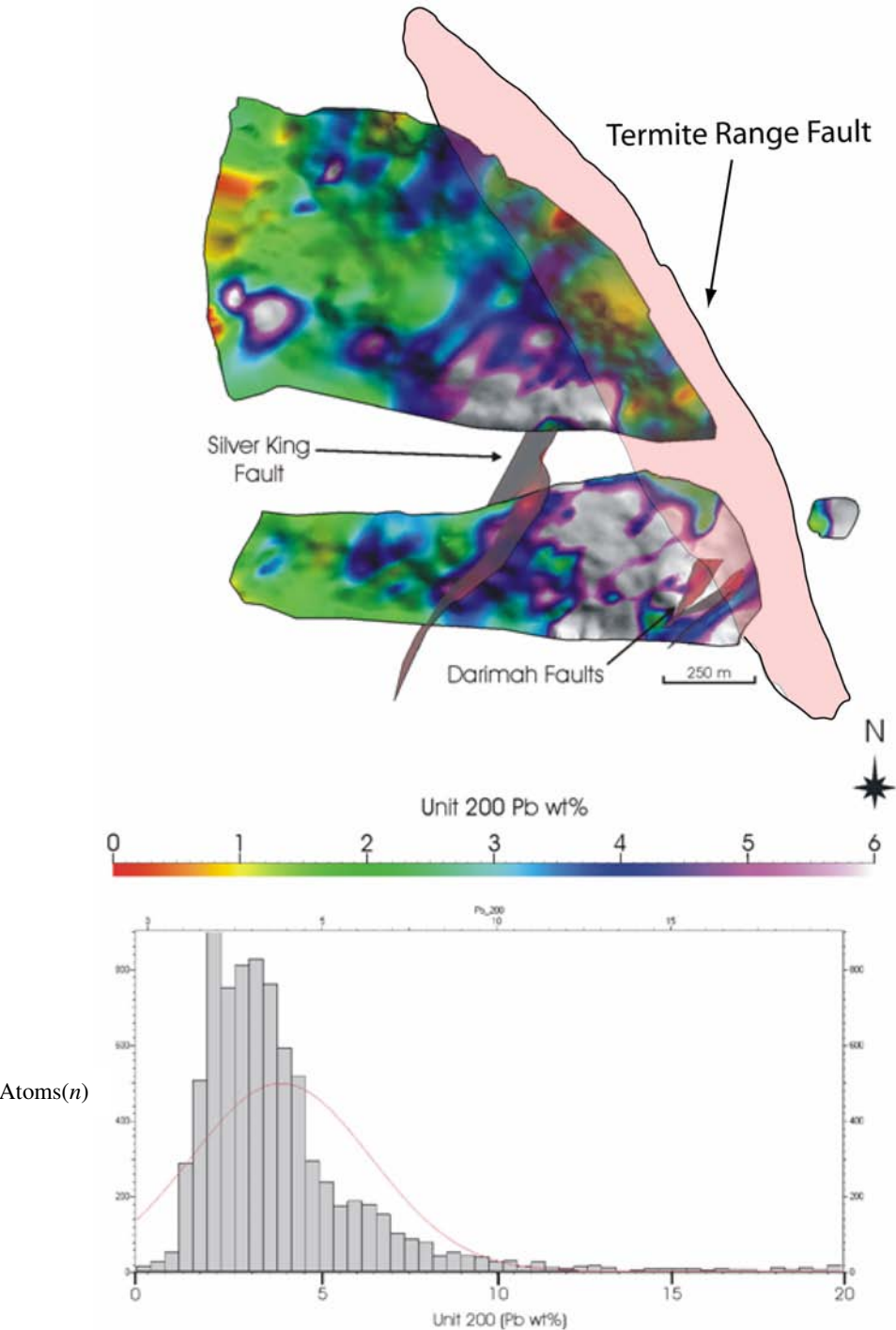
Fig. 4.11a 3D representation of the Pb distribution in Unit 200 of the Century deposit looking north. Note the correlation of higher grades with NE trending faults, and the spatial association of higher grade in the east (closer proximity to the Termite Range Fault). Below: Histogram displaying the Pb grade distribution of Unit 200.
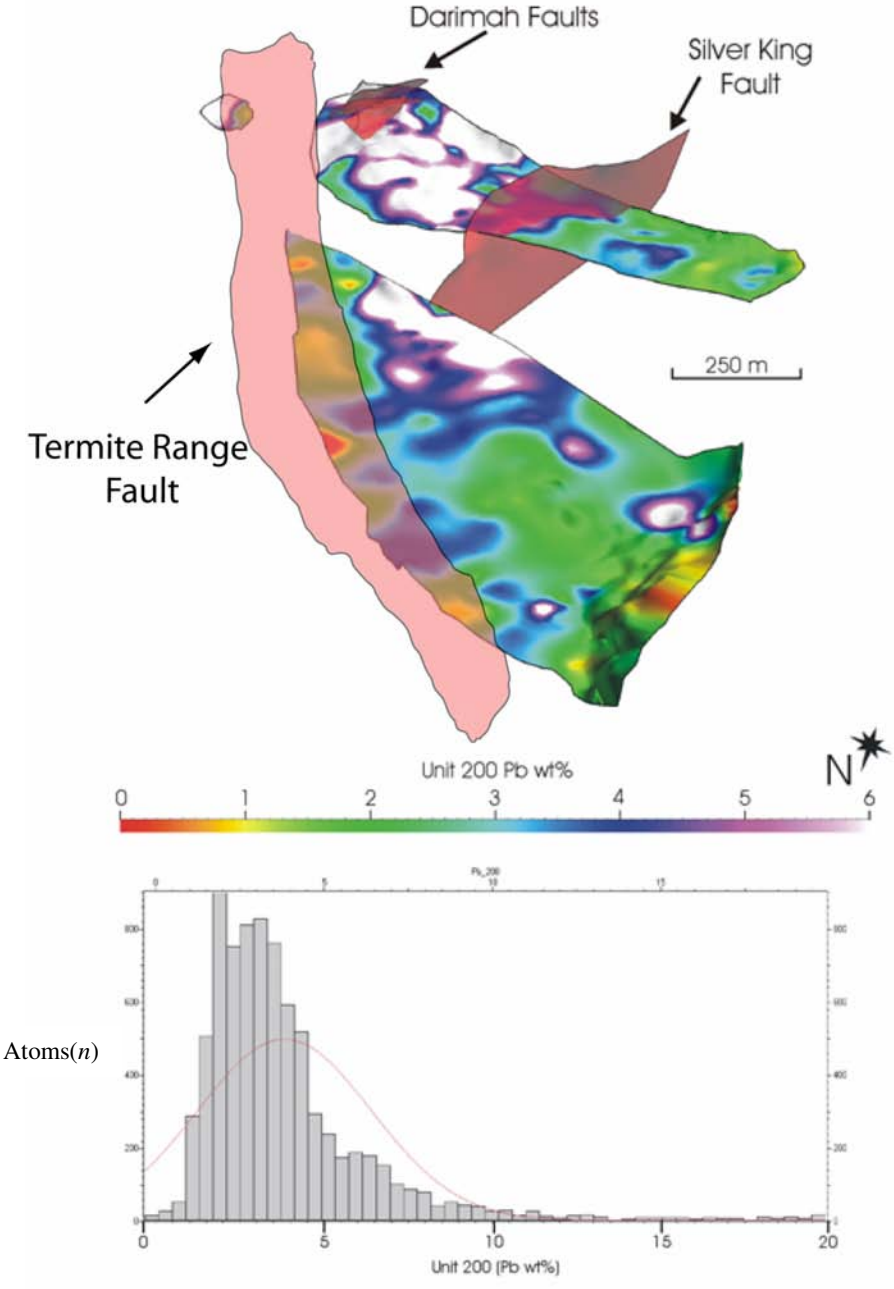
Fig. 4.11b. 3D representation of the Pb distribution in Unit 200 of the Century deposit looking south. Note the correlation of higher grades with NE trending faults, and the spatial association of higher grade in the east (closer proximity to the Termite Range Fault). Below: Histogram displaying the Pb grade distribution of Unit 200.
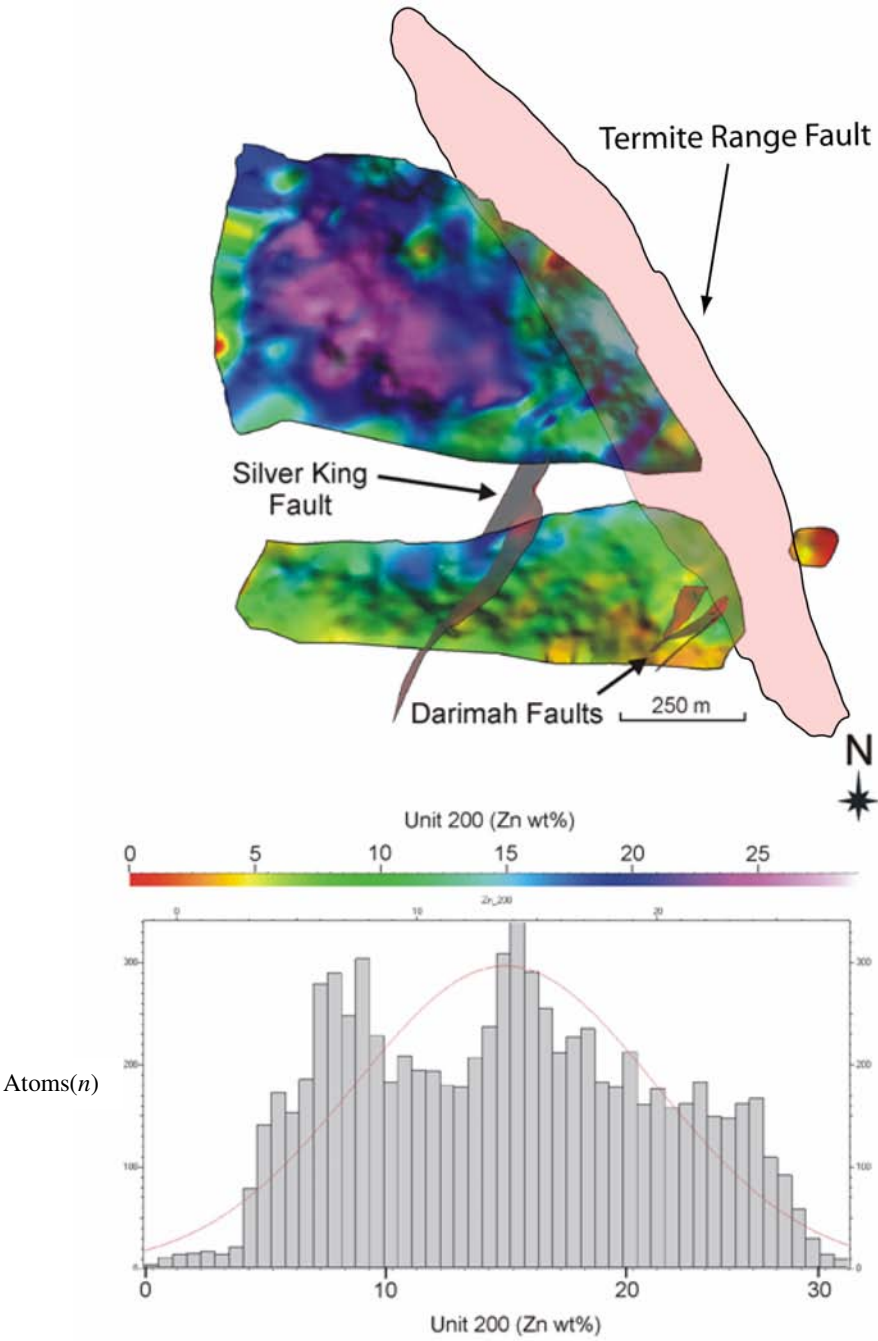
Fig. 4.12a. 3D representation of the Zn distribution in Unit 200 of the Century deposit looking north. Note the correlation of higher grades of Zn projecting along a NE trend, and the spatial distribution of higher grade in the west (distal to the Termite Range Fault). Below: Histogram displaying the Zn grade distribution of Unit 200.
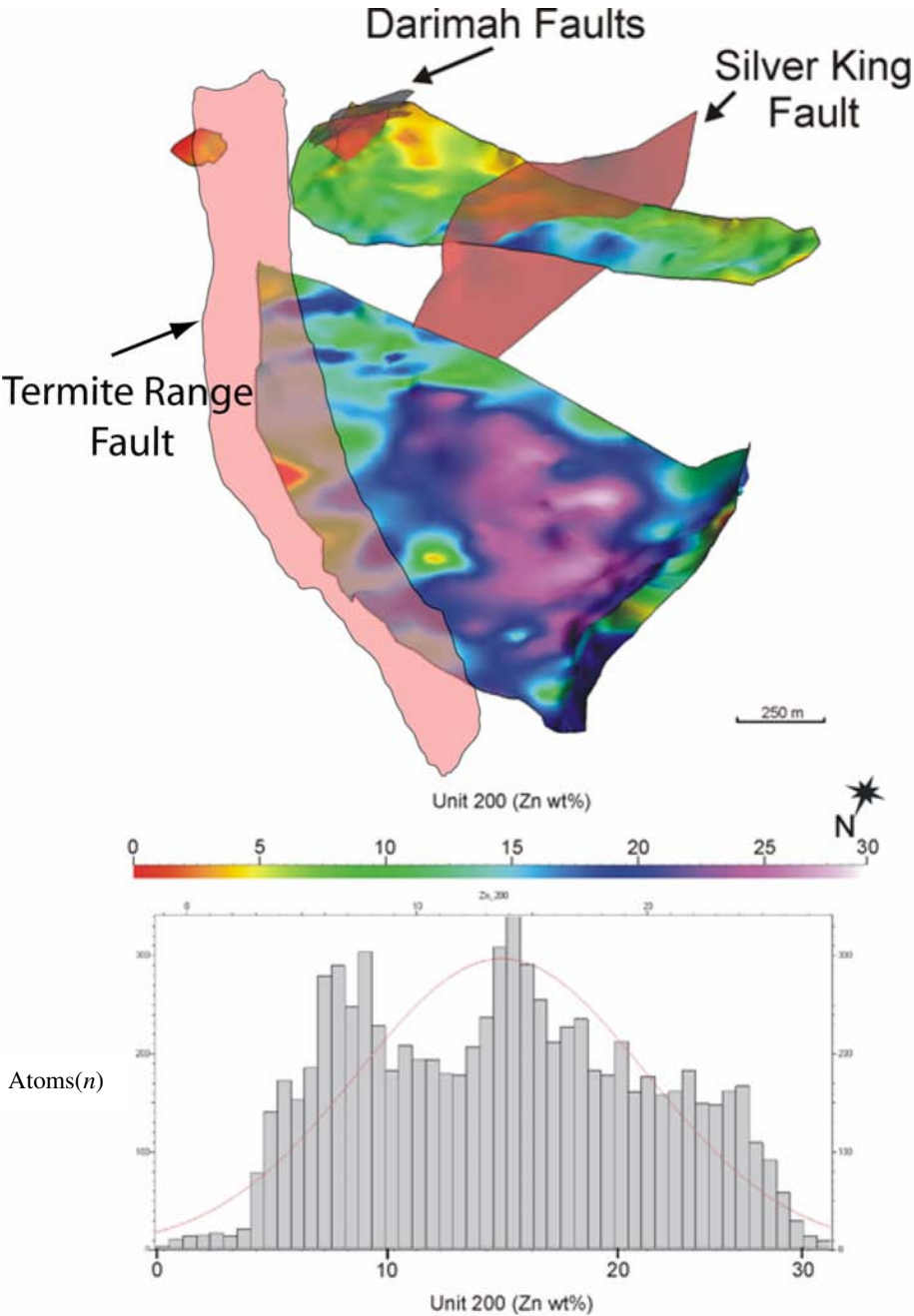
Fig. 4.12b 3D representation of the Zn distribution in Unit 200 of the Century deposit looking south. Note the correlation of higher grades of Zn projecting a NE trend, and the spatial association of higher grade in the west (distal to the Termite Range Fault). Below: Histogram displaying the Zn grade distribution of Unit 200.

To support his interpretation Broadbent (1999) describes a distinct relationship of sphalerite with pyrobitumen and further divides this relationship into upper and lower units within the mineralisation to underline the influence of the hydrocarbon reservoir phases, on textural aspects of the mineralisation. The lower part of the mineralised sequence contains 'porous sphalerite' (see Broadbent, 1999 for definition) which has a fine grained steel-grey appearance and a close association with pyrobitumen. In contrast, the upper part of the mineralised sequence is predominantly non-porous sphalerite consisting of almost pure sphalerite bands ranging from 0.2 to 5 mm in thickness. He concluded that a hydrocarbon source/reservoir represented a chemical trap for the mineralisation and contained an oil/gas interface that produced the different sphalerite textures. Cooke et al. (2003) noted however that both porous and non-porous sphalerite were interbedded throughout the deposit, although the proportions changed according to the gross zonation of Broadbent (1999). Broadbent et al. (1998), Broadbent, (1999) and Ord et al., (2002) also suggest that the hydrocarbon reservoir was overpressured at the time of mineralisation with consequent hydrofracturing and brecciation considered as main processes involved in fluid migration, metal leaching and deposition. Suggested metal sourcing for the Century system was related to clay transformation reactions from deeper units in the Lawn Hill Formation, and the conversion of sulphate to sulphide for metal precipitation as a result of thermochemical sulphate reduction (TSR) as the units passed through the 'oil window'.

4.6.   Deformation and Fluid Flow

Relationships between tectonic or geological settings and fluid flow are important in understanding potential sources and fluid pathways responsible for the formation of ore deposits. Common drivers for fluid migration include 1) topographic relief 2) 'squeegee' effects during thrusting and 3) deformation induced flow. The important effect of topographic relief and hydraulic head gradients has been well documented (e.g. Toth, 1962, 1963; Garven and Freeze, 1984a,b, Nesbitt and Muehlenbachs, 1989) and has been proposed as a significant hydrodynamic process with implications for long distance lateral fluid flow (e.g. Garven, 1985 – Mississippi Valley Type deposits). Oliver (1986) described the role of thrusting as a significant process in driving fluid flow in continental margins (the "squeegee" model), and in particular enabling lateral flow and the potential mixing of deep seated and surficial fluids in a contractional setting. Several authors have discussed at length the importance of deformation induced fluid flow (e.g. Etheridge et al., 1983, 1984; Cox, 1999; Ord and Oliver, 1997), which has a major influence over direction and rates of flow.

Compressional environments and inversion of compacted sedimentary basins typically lead to overpressurisation of pore fluids and upward fluid flow (e.g. Bethke, 1985; Upton, 1998) and Sibson (1987) has also linked upward flow and overpressurisation to fault valve activity. In extensional environments however, downward migration of fluids has been linked to the development of underpressure or where interconnectivity of fractures allows deep penetration of surface derived fluids (e.g. Nesbitt and Muehlenbachs, 1989; McLellan et al., 2004), and also in convection

cells (Simms and Garven, 2004). Broadbent (1999) considers overpressurisation as a primary mechanism for layer parallel fracturing, which allowed fluids to infiltrate the shale units and hence resulting in mineralisation. The majority of petroleum literature considers shale units to act as seals or caps, thus trapping fluids in aquifers such as sandstone. Broadbent (1999), however, concludes that the chlorite rich sandstone unit has acted as a seal and enabled overpressure in the shale unit below. He suggested that mechanically induced permeability of an otherwise low permeability unit, enabled lateral infiltration of metal rich fluids, which may have been transported up fault structures such as the TRF. Ord et al. (2002) presented coupled mechanical fluid flow and chemical models for the formation of the Century deposit, based primarily on Broadbent's (1999) interpretation. The main argument for these models, in a mechanical sense, is the preferential permeability assigned to the shale units, which reach a higher permeability than the faults transporting the mineralising fluids. In the context of the Century deposit, this leads to two potential scenarios for migration of fluids in relation to the genetic models presented previously, a syn-sedimentary/early diagenetic model and a syn-tectonic model; however lateral flow from major fluid pathways remains an issue. Here we aim to test possible scenarios for infiltration of fluids responsible for mineralisation by coupled deformation and fluid flow numerical simulations, by examining the potential types of faulting (growth faults and fault reactivation) present during the two most likely periods for mineralisation of the Century Zn-Pb-Ag deposit. The models within this study examine the potential for lateral flow within the shale units during extension and compression, and also the

permeability contrasts required to achieve this. The relationship between upward or downward migrating fluids and lateral fluid migration is also tested.

4.7.   Numerical modelling

The numerical models presented here are based on a coupled deformation and fluid flow approach, where mechanical deformation is the main driving force for fluid migration. To gain a better understanding and useful results, questions regarding the system under investigation must be posed. The main questions asked in this study are:

(1) What pathways controlled the location of favourable sites for mineralisation?

(2) What geological conditions were favourable for lateral fluid flow?

(3) What tectonic regimes were active and suitable for lateral flow?

(4) What role does overpressurisation have in controlling fluid flow and mineralisation?

4.7.1.   FLAC (Fast Lagrangian Analysis of Continua)

FLAC is a two-dimensional explicit finite difference modelling program, suitable for simulating the behaviour of geological materials that undergo plastic flow during yield (see Chapter 2). FLAC has been applied to many geological problems in Australia (e.g. Ord, 1991a,b; Ord and Oliver, 1997; Oliver et al., 2001, 2006; Upton et al., 1995, 1998; Upton, 1998; Zhang et al., 1996a,b, 2002; McLellan, 2000; McLellan et

al., 2004; Schaubs and Zhao, 2002). Materials are represented by zones that form a grid, which can be adjusted by the user to fit the geometry of the problem to be solved. Each zone within the grid can be prescribed properties (both elastic and plastic) and the zones behave according to a prescribed linear or non-linear stress/strain law as a response to applied forces. The material is allowed to yield and flow and deform whilst run in large-strain mode, and when in a coupled scenario, fluid allows interaction with and influence over this deformation. For a full description of FLAC see Chapter 2 and Appendix A.

4.7.2. Sensitivity of Strain Rates

As a result of rigorous sensitivity testing, strain rates within the FLAC models were found to be a critical parameter in determining not only pore pressure and hydraulic head distribution but also plasticity failure and ultimately fluid flow. Simulating deformation in FLAC can be done by either applying a boundary stress or a boundary velocity. In a Mohr-Coulomb constitutive relationship in FLAC there is no inherent time dependence associated with the mechanical steps, hence velocity boundary conditions are prescribed as a length per time step relationship, with real time only being associated with fluid steps in a coupled model. The unbalanced force in FLAC is a measure of equilibrium within the model grid and can represent a condition where we have steady state plastic flow. If the ratio of unbalanced force to internal forces within the model is large e.g. >1% then the boundary velocities are considered to be too great. In extensional deformation for example, we can check the effects of boundary velocities by examining the bulk extension rates of the model. This is done by

extracting information at specific grid points within the mesh and calculating the distance of movement and dividing this by the constitutive time of the model at this point. Typical values for geologically acceptable strain rates range from 1.00e-13 to 1.00e-17 sec^{-1} (e.g. Tadakazu et al., 2001; Pietrantonio and Riguzzi, 2004) and laboratory studies have shown strain rates as high as 1.00e-9 sec^{-1} (Turcotte and Schubbert, 2002). If strain rates are too slow then we have no plastic flow within the model, and if they are too great we have inertia effects and increased rates of deformation and fluctuating velocity histories. All models presented here have been tested for acceptable limits of bulk extension/shortening rates where applicable.

4.7.3. Conceptual models

Prior to any numerical modelling, an important step is to define the conceptual models and address the main questions posed in relation to the system under investigation. In this study two conceptual models are introduced in relation to the two possible fluid flow scenarios previously discussed, and linked to the tectonic setting that controls them. The conceptual models (Fig. 4.13a, b) consist of a 400 m by 400 m cross section representing a simplification of the mine stratigraphic intervals and the main geological components comprising the Century system (Fig. 4.14). The main aim of the constructed conceptual models is to explore the difference between a) extension and compression b) poorly consolidated materials and lithified materials (i.e. at depth) and c) permeability contrasts and hydrofracturing that may provide the potential for fluid to infiltrate the shale units in the Century system. Both models (extension and contraction)

are fully saturated with fluids, and pore pressure is initialised in Model 1 at hydrostatic, which represents conditions commensurate with early basin formation, and an overpressured zone is initialised in Model 2, which represents conditions commensurate with a later stage contraction. All physical properties are given in Table. 4.2.

Attempts were made to numerically model a syngenetic scenario, by prescribing all materials low values of elastic properties and in particular low cohesion values. However, unconsolidated sediments may not behave in a Mohr-Coulomb sense in reality (i.e. they may be poro-elastic, not elastic-plastic or poro-plastic). Not only might the constitutive properties be inappropriate, FLAC cannot simulate the effect of ongoing sedimentation. Finally, lowering the cohesion values produced extreme grid failure at low strains, confirming that FLAC was inappropriate for modelling this scenario. Thus, we consider only two subsurface genetic models, extension during basin evolution (diagenesis) and contraction during orogeny (epigenesis).
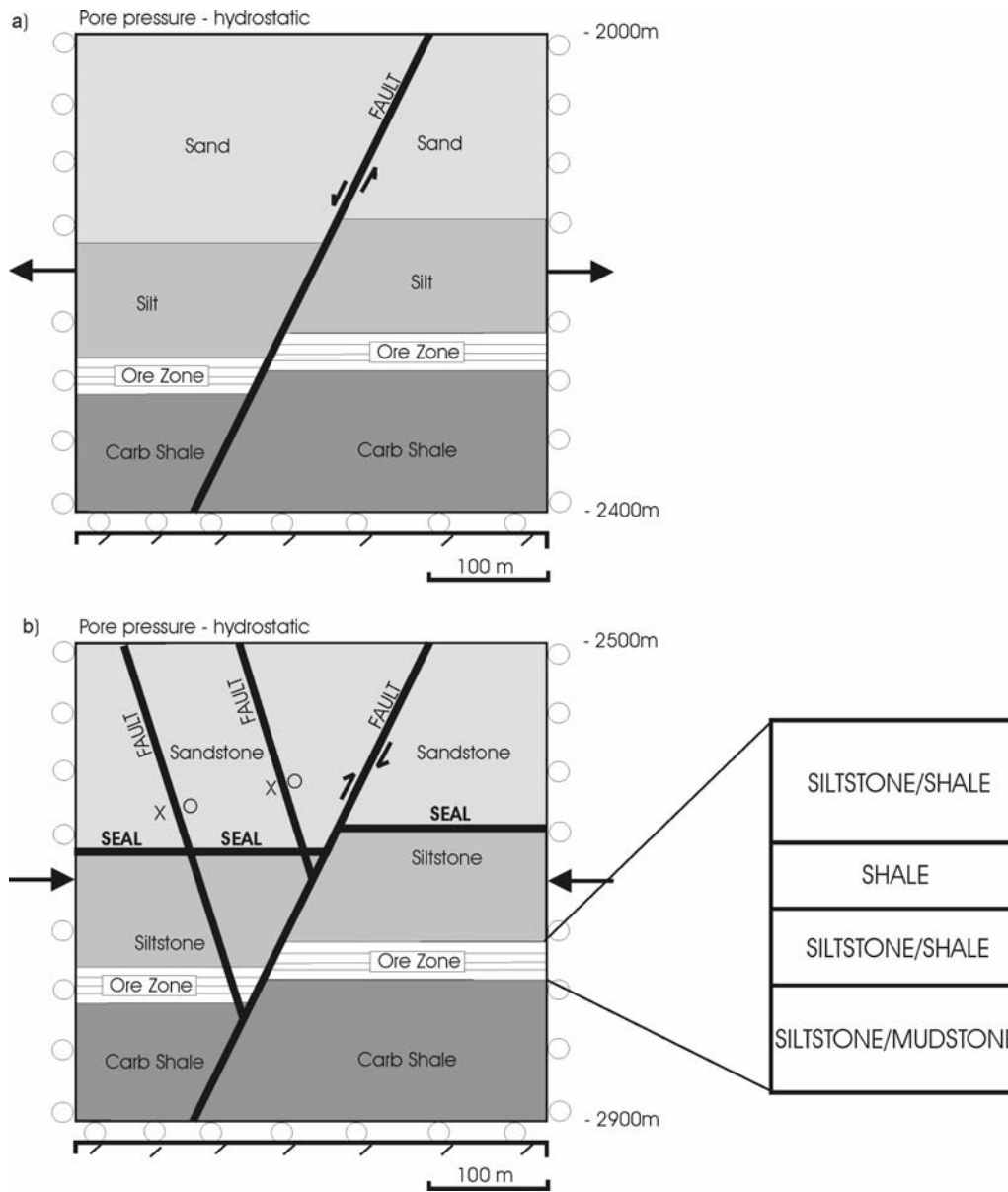
Fig. 4.13 Conceptual models for, a) Model 1 representing soft sediments and extensional deformation and b) Model 2 representing lithified sediments and later stage basin evolution. Ore Zone stratigraphy indicated. Model 2 has an overpressured zone applied in models 2b-d below the sandstone-siltstone interface at lithostatic pressures with the sandstone unit acting as a seal.
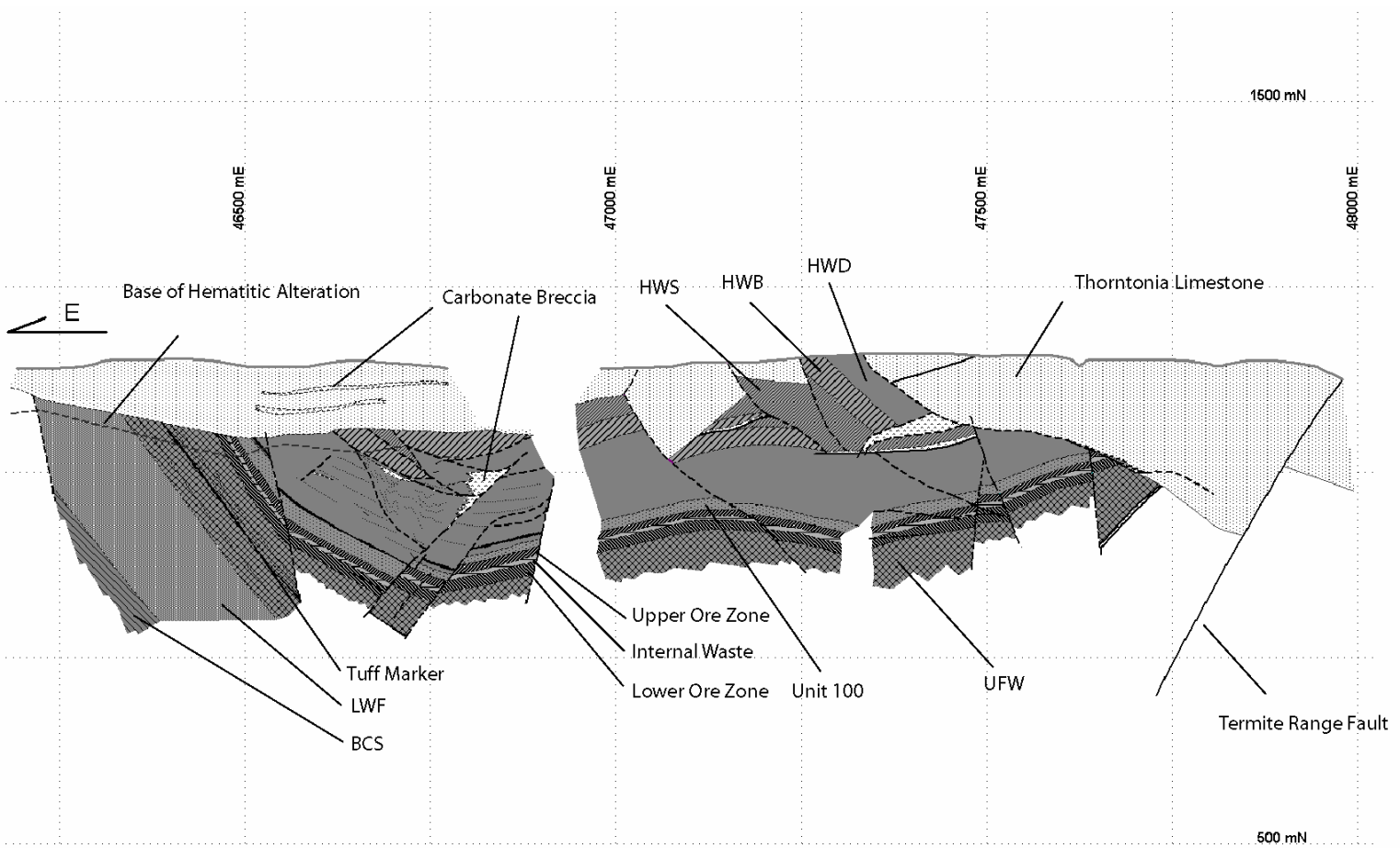
Fig. 4.14 Cross section of the Century deposit looking south, displaying the main structural features and stratigraphic elements. Note the Termite range Fault and its spatial relationship to parasitic faults to the east.

4.7.4. **Conceptual Model 1**

Conceptual model 1 (Fig. 4.13a) displays a simplified version of the mine stratigraphic units subdivision adopted after Kelso and Edge (unpublished report) (see Fig 4.7), and is cut by a normal fault, which represents the Termite Range Fault during and soon after sedimentation. Extensional deformation is applied to the model. The conceptual model represents an early diagenetic scenario in which sediments are considered to be semi-lithified, and here we are testing the effects of deformation and permeability contrasts on fluid flow.

To understand what permeability conditions are required to allow fluids to migrate through rock hosting the mineralisation, we tested two extensional models:

- **Model 1a** represents semi-lithified sediments and shale units (the most favourable host rock for Zn-Pb ore) with a low permeability value.

- **Model 1b** represents the same stratigraphy but the shales have higher permeability values to evaluate the permeability contrasts required to obtain significant fluid flow through them, and hence potential mineralisation.

Table 4.2 Physical properties for materials, Models 1 and 2.

Model	Density	Bulk modulus	Shear modulus	Cohesion	Friction angle	Dilation angle	Permeability
	(kg/m^3)	(Pa)	(Pa)	(Pa)	(°)	(°)	(m^2)
Model 1a							
Sand	1600	8.33e6	1.88e7	3.0e3	30	5	1.00e-12
Silt	1700	3.0e6	7.5e6	3.0e3	25	5	1.00e-13
All Shale	1800	3.33e5	5.01e6	1.0e3	20	2	1.00e-14
Silt / Shale	1750	8.0e5	7.0e6	2.0e3	22	3	5.00e-13
Silt / Mud	1750	8.0e5	9.5e5	2.0e3	22	3	2.00e-14
Fault	1600	3.33e5	7.0e4	1.0e3	20	5	1.00e-12

Model	Density	Bulk modulus	Shear modulus	Cohesion	Friction angle	Dilation angle	Permeability
	(kg/m^3)	(Pa)	(Pa)	(Pa)	(°)	(°)	(m^2)
Model 1b							
Sand	1600	8.33e6	1.88e7	3.0e3	30	5	1.00e-12
Silt	1700	3.0e6	7.5e6	3.0e3	25	5	1.00e-13
Carbonaceous Shale	1800	3.33e5	5.01e6	1.0e3	20	2	1.00e-14
Ore Shale	1800	3.33e5	5.01e6	1.0e3	20	2	1.00e-12
Silt / Shale	1750	8.0e5	7.0e6	2.0e3	22	3	5.00e-13
Silt / Mud	1750	8.0e5	9.5e5	2.0e3	22	3	2.00e-14
Fault	1600	3.33e5	7.0e4	1.0e3	20	5	1.00e-12

Model	Density	Bulk modulus	Shear modulus	Cohesion	Friction angle	Dilation angle	Permeability
	(kg/m^3)	(Pa)	(Pa)	(Pa)	(°)	(°)	(m^2)
Models 2a-b							
Sandstone	2400	2.68e10	7.0e9	2.7e7	27	4	1e-15 to 1e-19
Siltstone	2450	1.56e10	1.08e10	3.47e7	25	4	1.00e-16
Ore Shale	2500	8.8e9	4.3e9	3.84e7	14	2	1.00e-19
Carbonaceous Shale	2500	8.8e9	4.3e9	3.84e7	14	1	1.00e-19
Siltstone / Shale	2500	1.0e10	7.5e9	3.6e7	23	2	5.00e-16
Siltstone / Mudstone	2600	1.0e10	7.5e9	3.6e7	23	2	1.00e-18
Fault	2300	4.70e9	4.30e9	8.00e5	30	5	1.00e-14

note: Model 2b decreases permeability of Sandstone to 1.00e-19 and overpressure is applied

Model	Density	Bulk modulus	Shear modulus	Cohesion	Friction angle	Dilation angle	Permeability
	(kg/m^3)	(Pa)	(Pa)	(Pa)	(°)	(°)	(m^2)
Models 2c-d							
Sandstone	2400	2.68e10	7.0e9	2.7e7	27	4	1e-15 to 1e-19
Siltstone	2450	1.56e10	1.08e10	3.47e7	25	4	1.00e-16
Ore Shale	2500	8.8e9	4.3e9	3.84e7	14	2	1.00e-15
Carbonaceous Shale	2500	8.8e9	4.3e9	3.84e7	14	1	1.00e-19
Siltstone / Shale	2500	1.0e10	7.5e9	3.6e7	23	2	5.00e-16
Siltstone / Mudstone	2600	1.0e10	7.5e9	3.6e7	23	2	1.00e-18
Fault	2300	4.70e9	4.30e9	8.00e5	30	5	1.00e-14

note: Model 2b has an additional yield function applied

4.7.5.   Conceptual Model 2

The second conceptual model (Fig. 4.13b) is similar to Model 1; however two additional parasitic faults have been added to reflect the evolution of the Termite Range Fault, which appears to have been reactivated during syn- to post-tectonic deformation. The stress applied to this second conceptual model is consistent with compression. In this case it is intended to represent a later stage of evolution of the Century system in which fluids are more tectonically driven with major topographic and deformation induced flow. Within this compressional model we test four alternative scenarios:

- **Model 2a** has regular rehological properties assigned for the appropriate rock types;

- **Model 2b** then assigns a low permeability to the sandstone unit (as described earlier) with a decrease in permeability from 1e-15 to 1e-19 m2, and the role of overpressure is investigated following the hypothesis proposed by Broadbent et al. (1998);

- **Model 2c** is also initialised with an overpressured area at the siltstone/sandstone boundary in correspondence with the interpretation of Broadbent (1999), and has an increase in permeability of the shale units from 1e-19 to 1e-15 m2; and

- **Model 2d** introduces an additional function that increases permeability by 10% within the model when materials are at yield and returning to or retaining their original permeability when not at yield. This function

allows deformation induced permeability to be investigated in the shale units and other rocks and faults.

4.8.   Results

Initial models (Model 1a and 1b) were constructed with assigned material properties conducive to semi-lithified sediments (i.e. relatively low cohesion), and as a consequence, the model grid fails shortly following 2% extension. However, initial results during early periods of extension in these models are presented. Models 2a-d represent lithified rocks (higher cohesion) and are deformed to around 12% shortening. The results of all models are presented below.

4.8.1.   Model 1a (extension, semi-lithified sediments, low permeability shale)

At very early stages of extension (1%) fluid flow is primarily focussed within the fault, sandstone and silt layers, due to higher permeability of these units (Fig. 4.15a). Local pore pressure gradients intensify fluid flow with maximum flow velocities of 1.44e-8 m/s^{-1} (0.45 m/yr^{-1}). On closer inspection fluid can be seen to be drawn from the fault into the siltstone layers with an overall flow direction from left to right, however little to no flow is evident within the shale as a result of the low permeability values assigned to these units (Fig. 4.15b). At around 2% extension pore pressure has decayed slightly, displaying supra-hydrostatic pore pressures and a sub-hydrostatic

gradient (Fig. 4.16a). Fluid flow is more evident within the more permeable units of sandstone, siltstone and within the fault, with increased flow velocities of 1.704e-8 m/s^{-1} (0.54 m/yr^{-1}) (Fig. 4.16b).

As a result of the low values in elastic properties of the sediments, the model grid fails soon after 2% deformation. If ore deposition occurred in zones of high fluid flux, it would have been most concentrated in the faults and coarser grained sediments, according to this model.

4.8.2. Model 1b (extension, semi-lithified sediments, high permeability shale)

As with Model 1a, initial extension causes perturbations in fluid flow which is primarily driven by pore pressure gradients (Fig. 4.17a). Unlike Model 1a however, strong lateral flow can be seen in the shale units due to the assigned permeability being similar to the fault and greater than the surrounding sediments (Fig. 4.17b). As pore pressure decays as a result of extension similar patterns to Model 1a are evident, with downward migrating fluid primarily within the more permeable fault and lateral flow within the stratigraphic units (Fig. 4.18). Comparative increases in fluid flow velocities to Model 1a are seen as a result of continuing deformation from 1 to 2% extension (1.475e-8 m/s^{-1} to 1.788e-8 m/s^{-1} – 0.47 m/yr^{-1} to 0.56 m/yr^{-1}). According to this model, substantial fluid flow may have caused mineralisation in shales and faults. Inflow towards the fault or outflow away, along the shale layers, is dependent on detail of the geometry chosen.
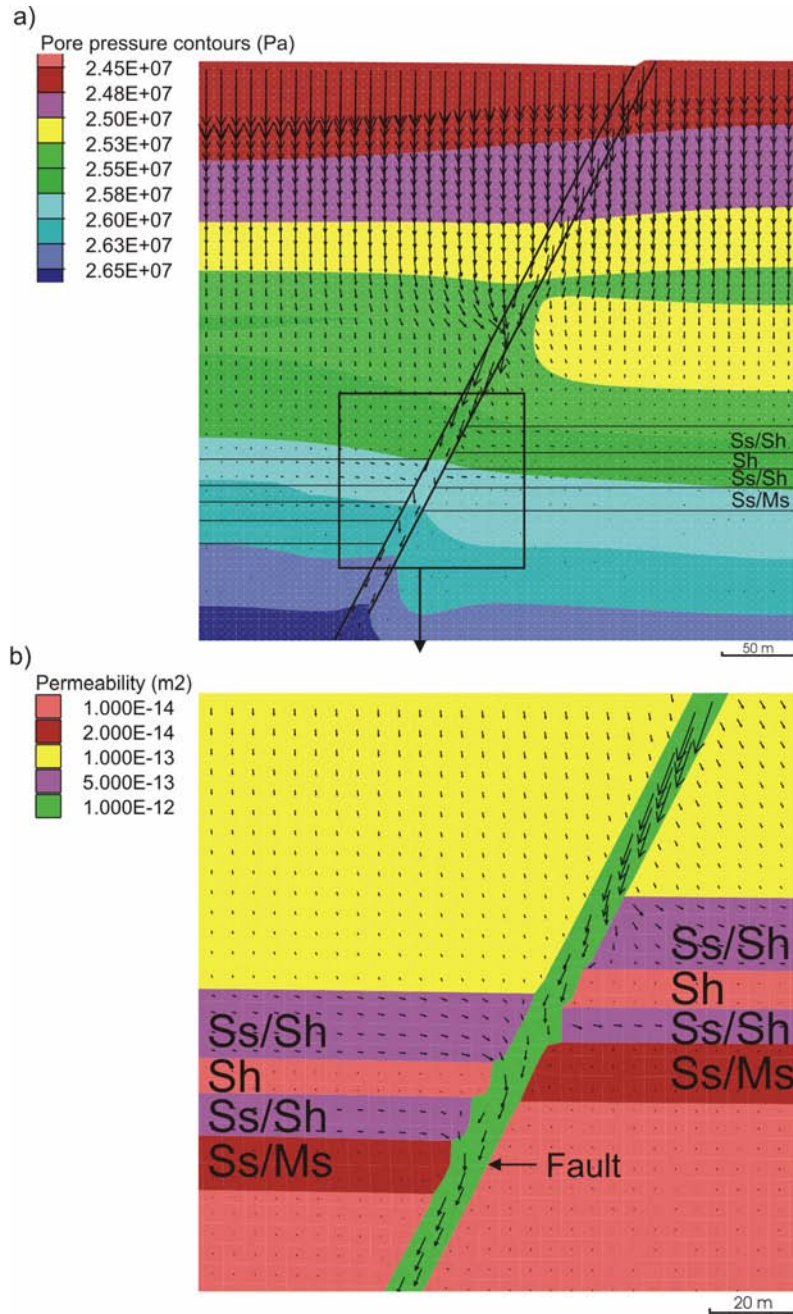
Fig. 4. 15 Model 1a showing plots of a) pore pressure contours and Darcy fluid flow vectors for Model 1a at 1% extension, displaying predominant downward migration of fluids within the more permeable fault and sediments, b) magnified plot of the ore zone displaying permeability values and flow vectors. Note the lack of fluid flow within the shale units.
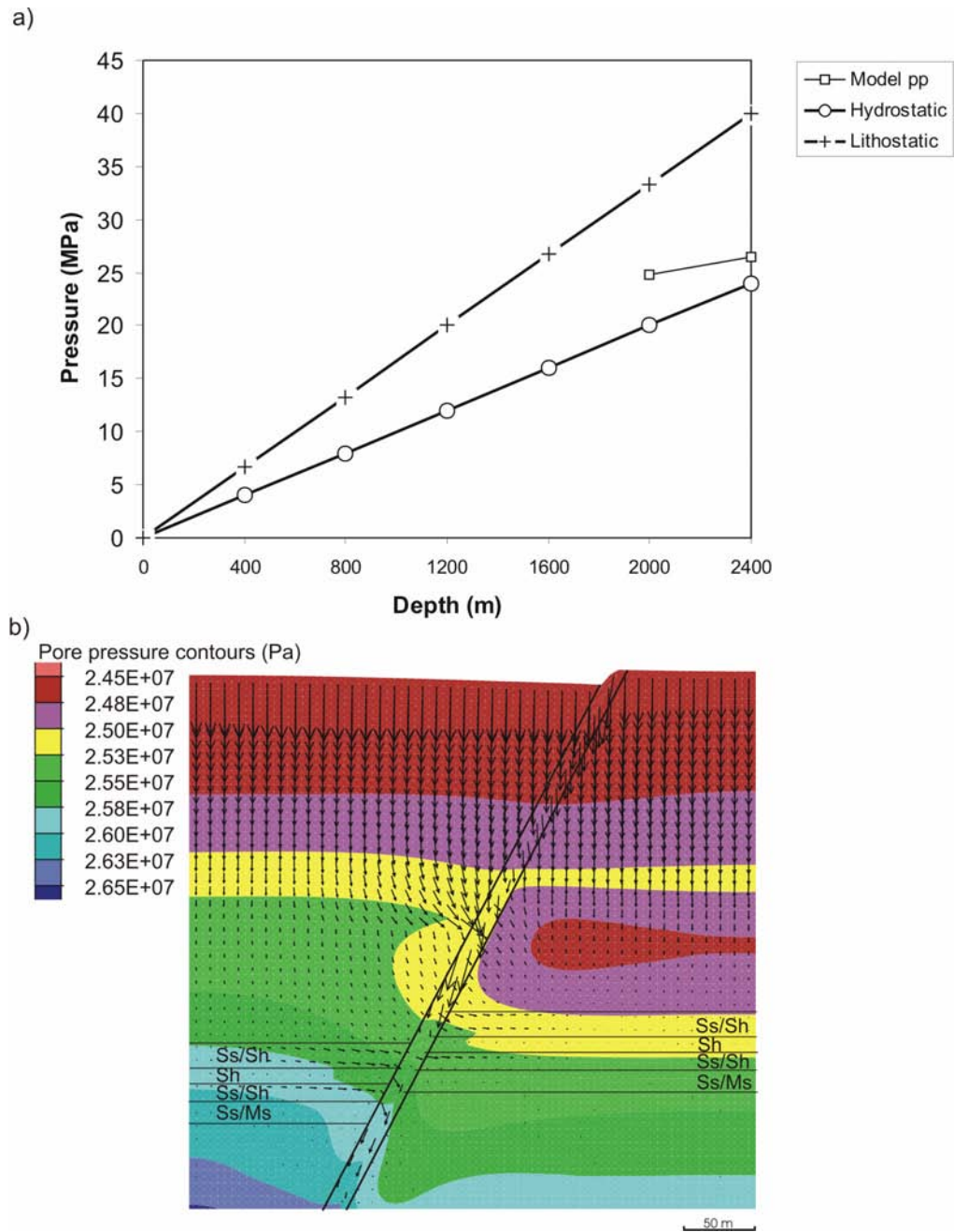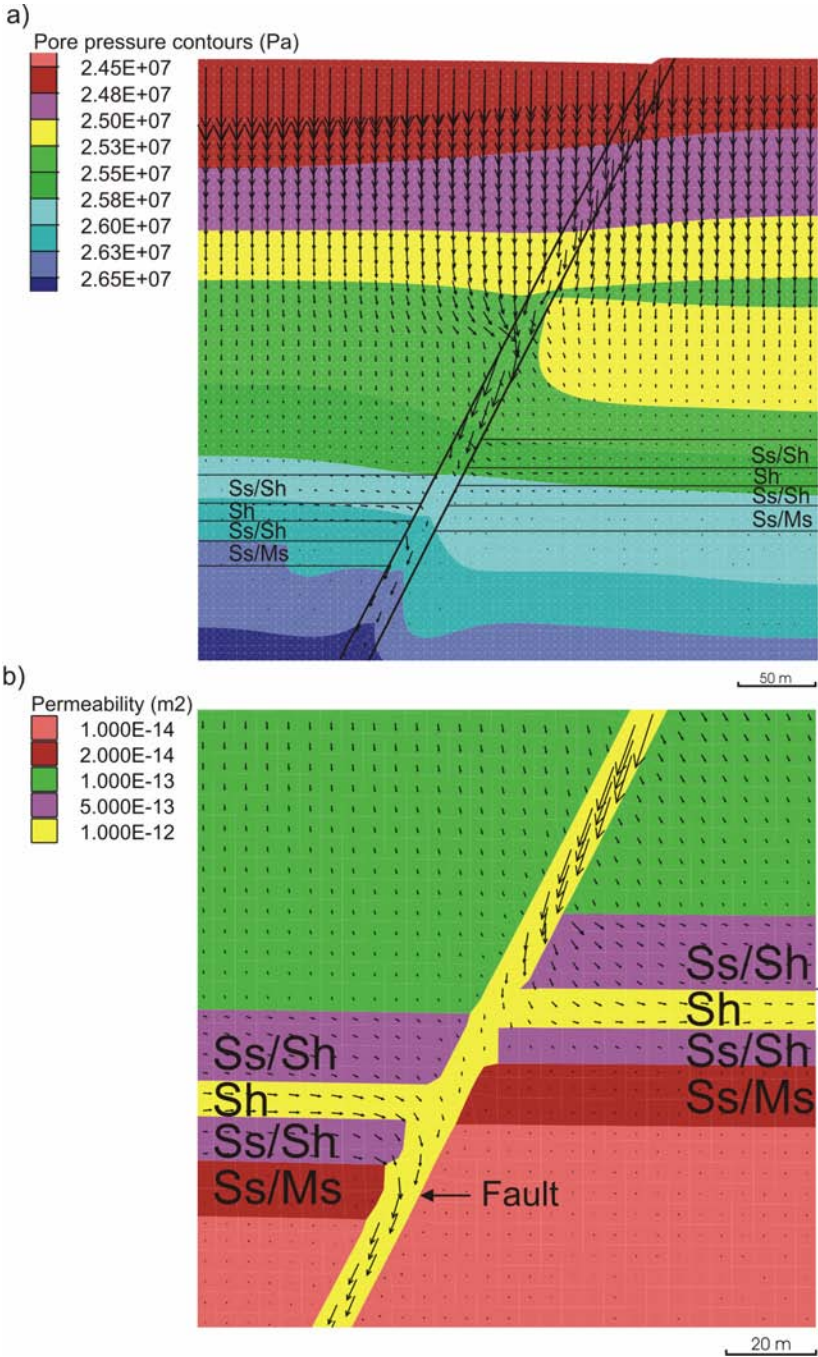
a)

b)

Fig. 4. 16 Model 1a at around 2% extension, a) depth v pressure graph illustrating pore pressure decay due to extension, displaying supra-hydrostatic pore pressures and a sub-hydrostatic gradient, b) plot of pore pressure and Darcy fluid flow vectors indicating an overall downward trend of fluid flow within the fault and lateral flow in the more permeable siltstone layers.

Fig. 4.17 Plot of a) pore pressure contours and Darcy fluid flow vectors for Model 1b at 1% extension, displaying predominant downward migration of fluids within the more permeable fault and sediments, b) magnified plot of the ore zone displaying permeability values and flow vectors. Note the strong fluid flow within the shale units (yellow).
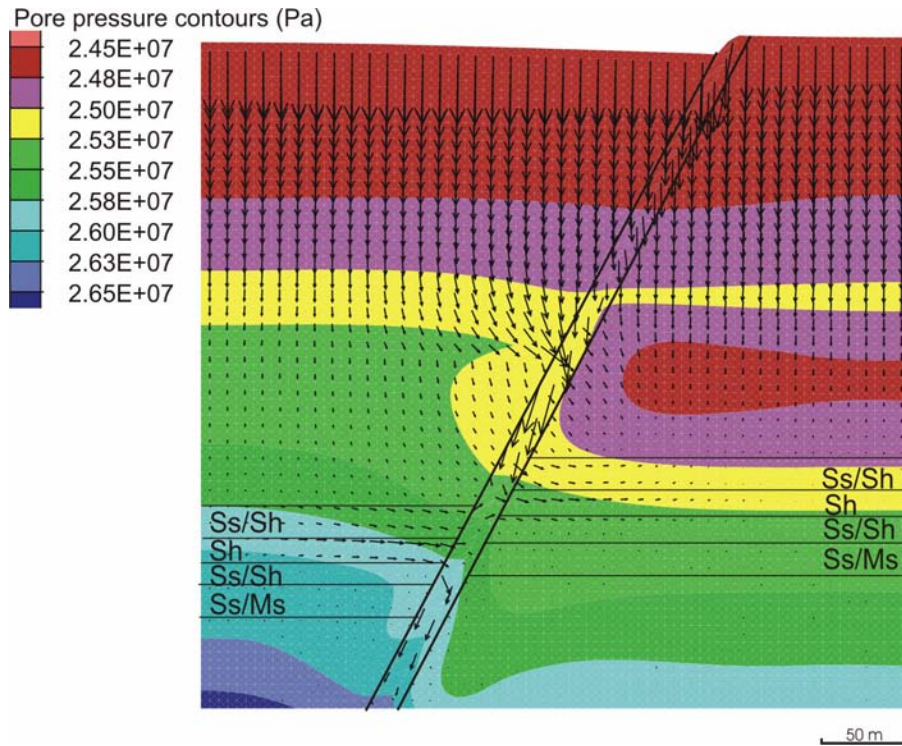
Fig. 4.18 Plot of pore pressure contours and Darcy fluid flow vectors for Model 1b at 2% extension, displaying predominant downward migration of fluids within the more permeable fault and sediments, and strong lateral fluid flow within the shale units.

In summary, the results from the simulation of semi-lithified sediments and poorly consolidated material indicate that FLAC has difficulty in modelling material of this type, due to inadequate constitutive models and grid failure. However, useful results for some models are indicated in very early stages of extension, where fluid flow is focussed within more permeable material and driven by initial changes in pore pressure gradients and permeability contrasts. When the shale unit within the 'ore zone' has permeability values as high as to less than one order of magnitude lower than that of the fault, notable fluid flow is evident in shales, which may indicate the potential for a

diagenetic replacement in a subsurface condition. The permeability is one of the primary factors that control fluid flow, during early stages of diagenesis.

4.8.3. Model 2a (contraction, low permeability shale)

A significant difference from the previous models discussed is that within this model fluid is focussed within the fault in an overall upward migration path (Fig. 4.19a). This was achieved by an initial compression, resulting in an increase in pore pressure (up to 75 MPa) within the model that forces fluid up the more permeable fault. Pore pressure cycles due to deformation and the system responds (Fig. 4.19b). The shale unit contains isolated areas of high pore pressure in comparison to other units as a result of the shale's low permeability and low dilation angle (Fig. 4.20a). Areas of dilation are observed within the model as deformation progresses (10% shortening), in particular to the left of the main fault, although focussing of fluids remains concentrated within the more permeable faults (Fig. 4.20b). The faults, however, show local contractional behaviour and limit fluid flow nearer the top of the model. Due to the limited permeability and lack of dilation in the shale units, no significant fluid flow is noted within them (Fig. 4.21).
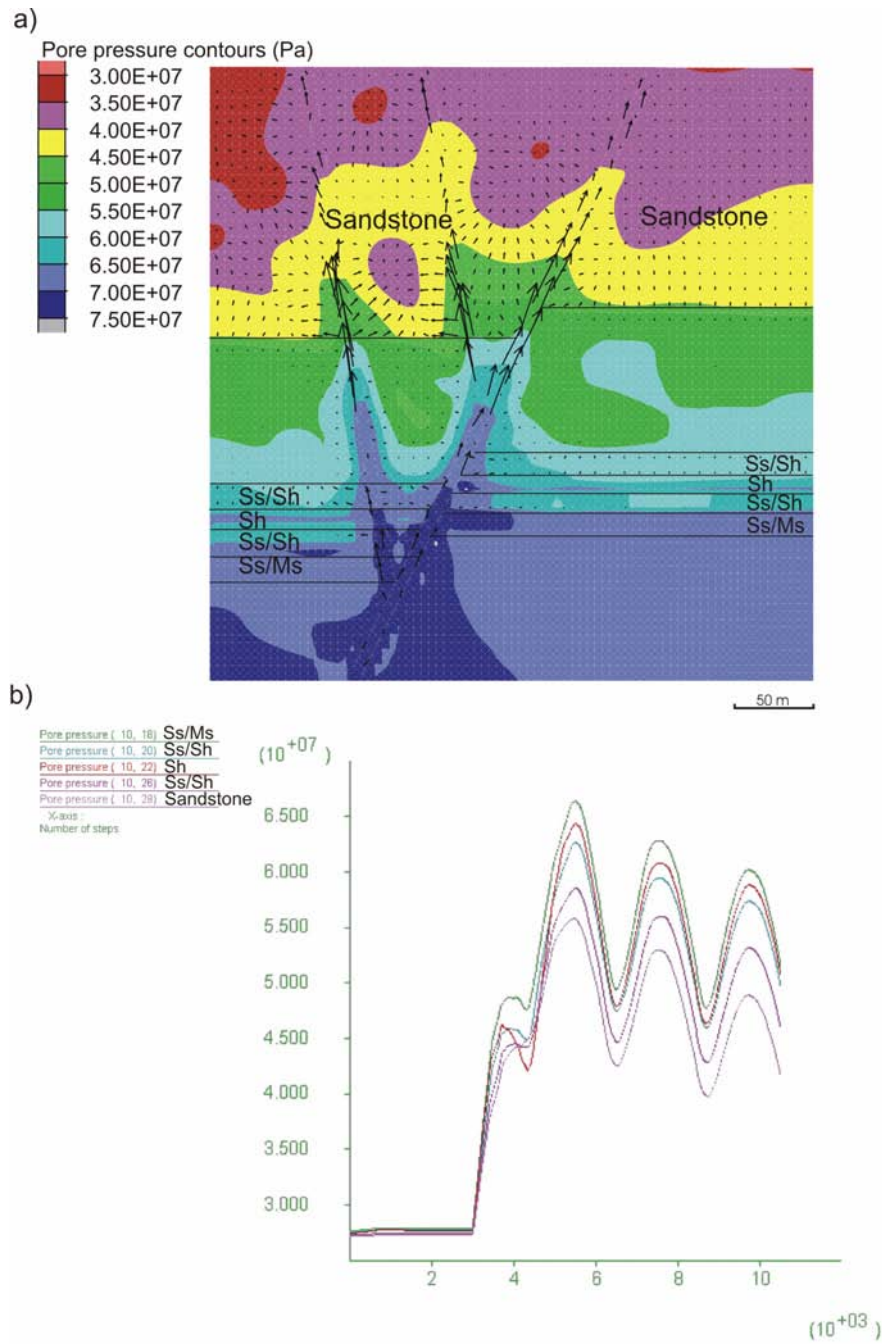
a)

Pore pressure contours (Pa)

	3.00E+07
	3.50E+07
	4.00E+07
	4.50E+07
	5.00E+07
	5.50E+07
	6.00E+07
	6.50E+07
	7.00E+07
	7.50E+07

Sandstone   Sandstone

Ss/Sh
Sh
Ss/Sh
Ss/Ms

Ss/Sh
Sh
Ss/Sh
Ss/Ms

50 m

b)

Pore pressure (10, 18) Ss/Ms
Pore pressure (10, 20) Ss/Sh
Pore pressure (10, 22) Sh
Pore pressure (10, 26) Ss/Sh
Pore pressure (10, 29) Sandstone
X-axis :
Number of steps

(10^{+07})

6.500
6.000
5.500
5.000
4.500
4.000
3.500
3.000

2   4   6   8   10

(10^{+03})

Fig. 4.19 Early stages of compression for Model 2a, a) plot of pore pressure and Darcy fluid flow vectors indicating an overall upward trend of fluid flow within the fault and very limited lateral flow in the permeable siltstone layers b) graph of pore pressure v time, illustrating pore pressures in all units from the over zone to the sandstone. Note the cyclic behaviour of pore pressure due to deformation.
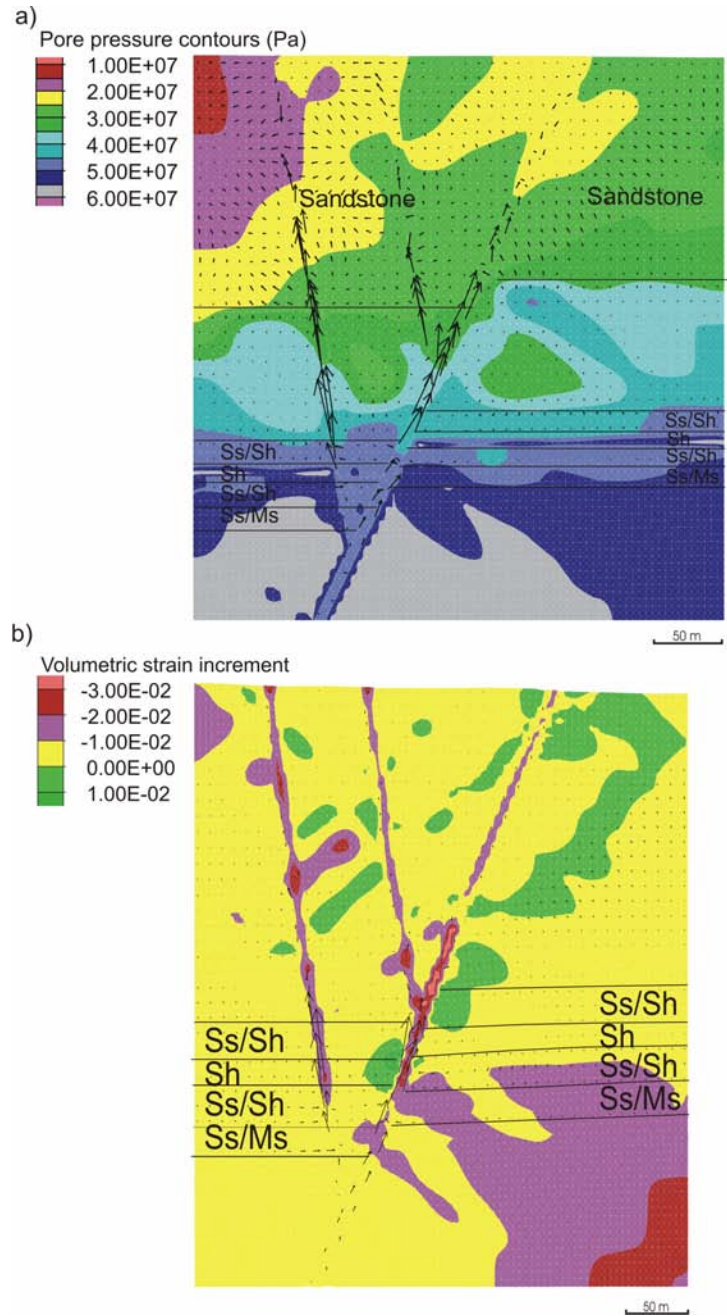
Fig. 4.20 Early to late stages of compression for Model 2a, a) 3% compression, plot of pore pressure and Darcy fluid flow vectors indicating an overall upward trend of fluid flow within the fault and very limited lateral flow in the permeable siltstone layers b) 9% compression, plot of volumetric strain (dilation) and Darcy fluid flow vectors indicating an overall upward trend of fluid flow within the fault and limited lateral flow in the permeable siltstone layers. Most dilation is occurring close to the fault structures.

Fig. 4.21 Late stage of compression (9%) for Model 2a, plot of volumetric strain (dilation) and Darcy fluid flow vectors indicating an overall upward trend of fluid flow within the fault and insignificant flow within the shale layers.

4.8.4. Model 2b (contraction, low permeability shale and sandstone, with overpressure)

In simulating the sandstone unit at the top of the model as a 'cap' or 'seal' to the system, the permeability of this unit is reduced. An overpressure is applied at the base of the sandstone unit and over the ore zone in agreement with the model proposed by Broadbent (1998) and Ord et al. (2002), as the chlorite rich sandstone has been interpreted as a seal in the system. As deformation commences, fluid is forced through the seal and into the faults penetrating above the sandstone (Fig. 4.22a-d). As compression progresses (3% shortening) strong upward flow driven by pore pressure gradients is seen within the fault structures (Fig. 4.23a). At around 5% shortening, dilational zones are prominent within the middle regions of the model and appear to be closely related to areas bounding faults (Fig. 4.23b). As deformation continues fluid flow continues upwards within the more permeable faults, with lesser flow noted within the siltstone layers and no flow in the shale layers (Fig. 4.24). Dilation is prominent as a band within the centre of the model; however this has no major influence on focussed fluid flow.
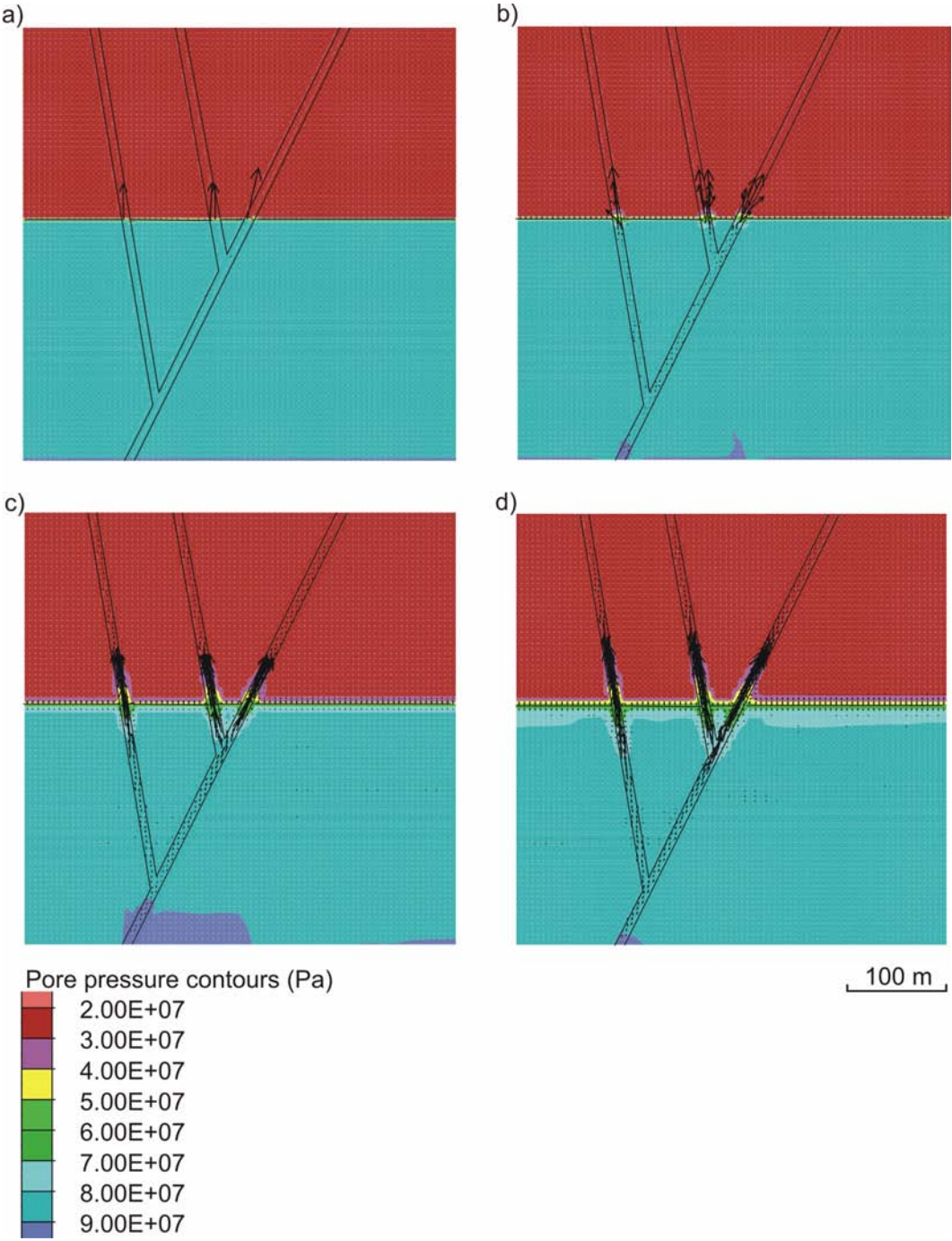
Fig. 4.22 Model 2b at commencement of deformation and release of overpressure, a) to d) representing stages of this process showing pore pressure contours forcing fluid upwards through the fault system with no lateral fluid flow evident.
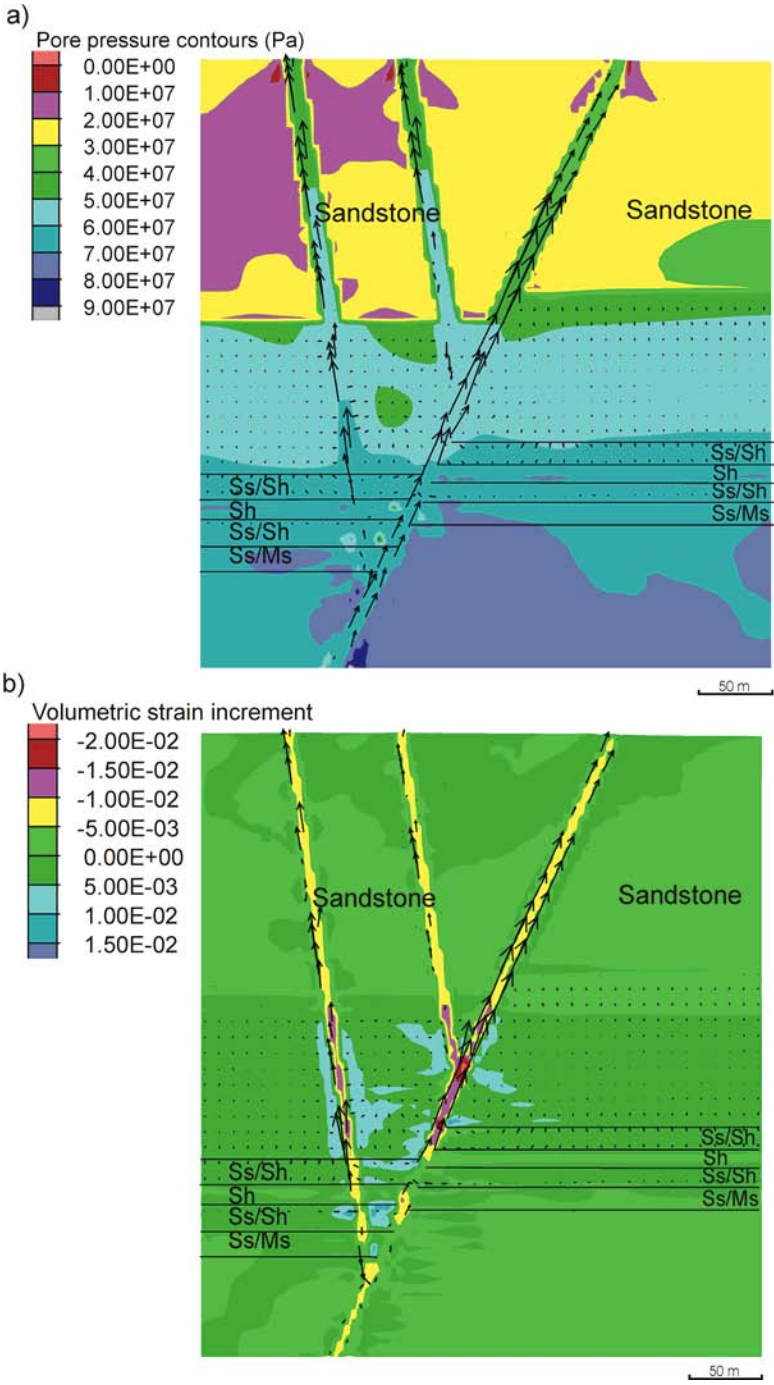
Fig. 4.23 Model 2b at a) 3% deformation, displaying pore pressure contours and a strong Darcy fluid flow focussing within the fault zones and b) 5% deformation, plot of volumetric strain (dilation) and Darcy fluid flow vectors, displaying strong flow within the faults and minor lateral flow in the siltstone layers.
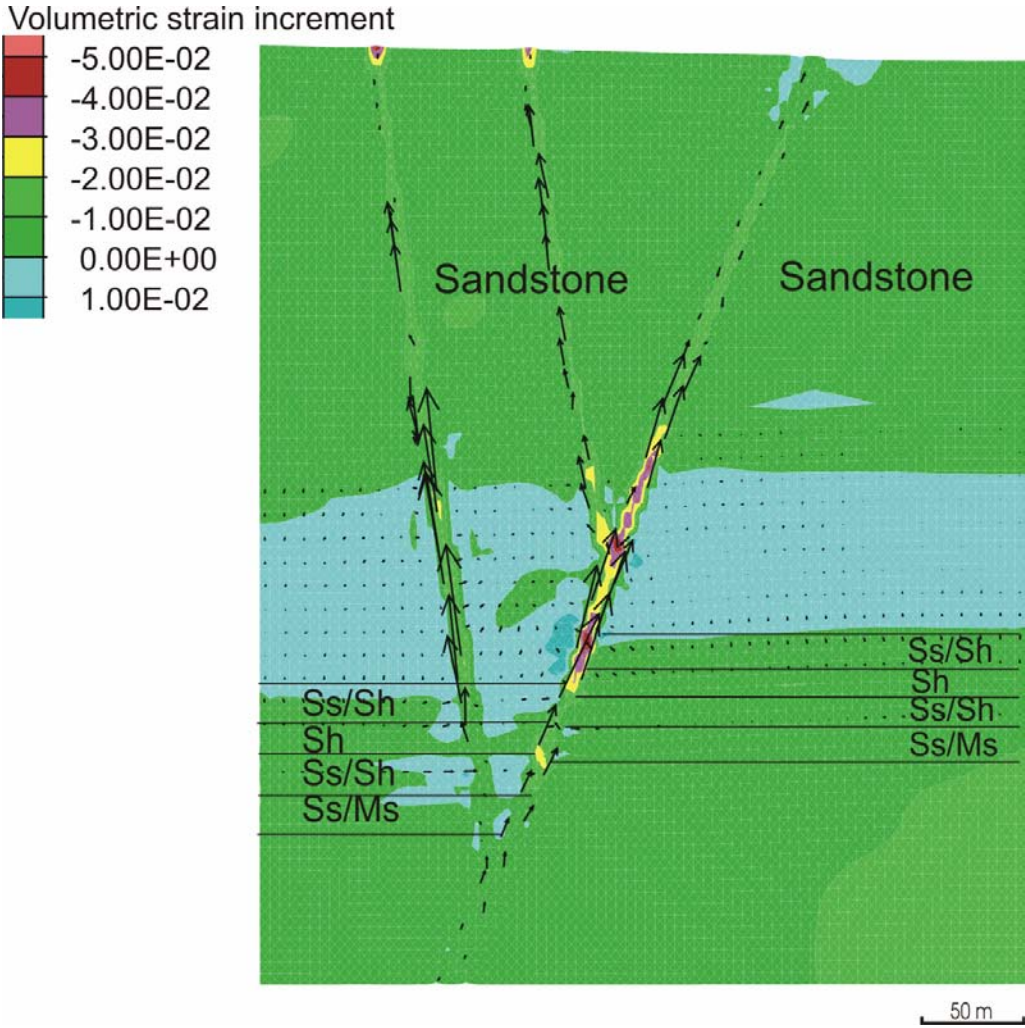
Fig. 4.24 Model 2b at 9% compression displaying volumetric strain (dilation) and Darcy fluid flow vectors. Dilation is primarily associated with a band in the centre region of the model and around fault structures.

4.8.5.   Model 2c (contraction, high permeability shale, low permeability sandstone, with overpressure)

Increasing the permeability of the shale units within the 'ore zone' has a major effect on fluid flow within this unit. At early stages of deformation (1% shortening) fluid flow is focussed in an upward direction within the more permeable faults, and lateral flow is evident from the fault into the shale units (Fig. 4.25a). Areas of high pore pressures are apparent from the base of the main fault (Fig. 4.25b) which is forcing fluid up the fault structures. Corresponding dilational zones are evident in close proximity to fault structures below the sandstone and siltstone interface, and in particular are found between the lower branching fault and the main fault (Fig. 4.26a). As deformation progresses, focussed flow within the shale unit is more apparent, with fluid being drawn from the shale units towards the faults. As deformation continues (5% shortening), fluid flow is preferentially focussed along the shale units and is also driven upwards through the permeable faults (Fig. 4.26b). Very limited fluid flow or dilation is seen within the sandstone, and it maintains overpressure in the units below, allowing only the fault structures to dissipate pressure up the faults. Within this model overall, pore pressure decays towards an equilibrium state following the release of the overpressure, and it is primarily driven by deformation and dilatancy. According to this model, if ore grades were related primarily to large fluid fluxes, shale units between the feeder faults would show high grades.
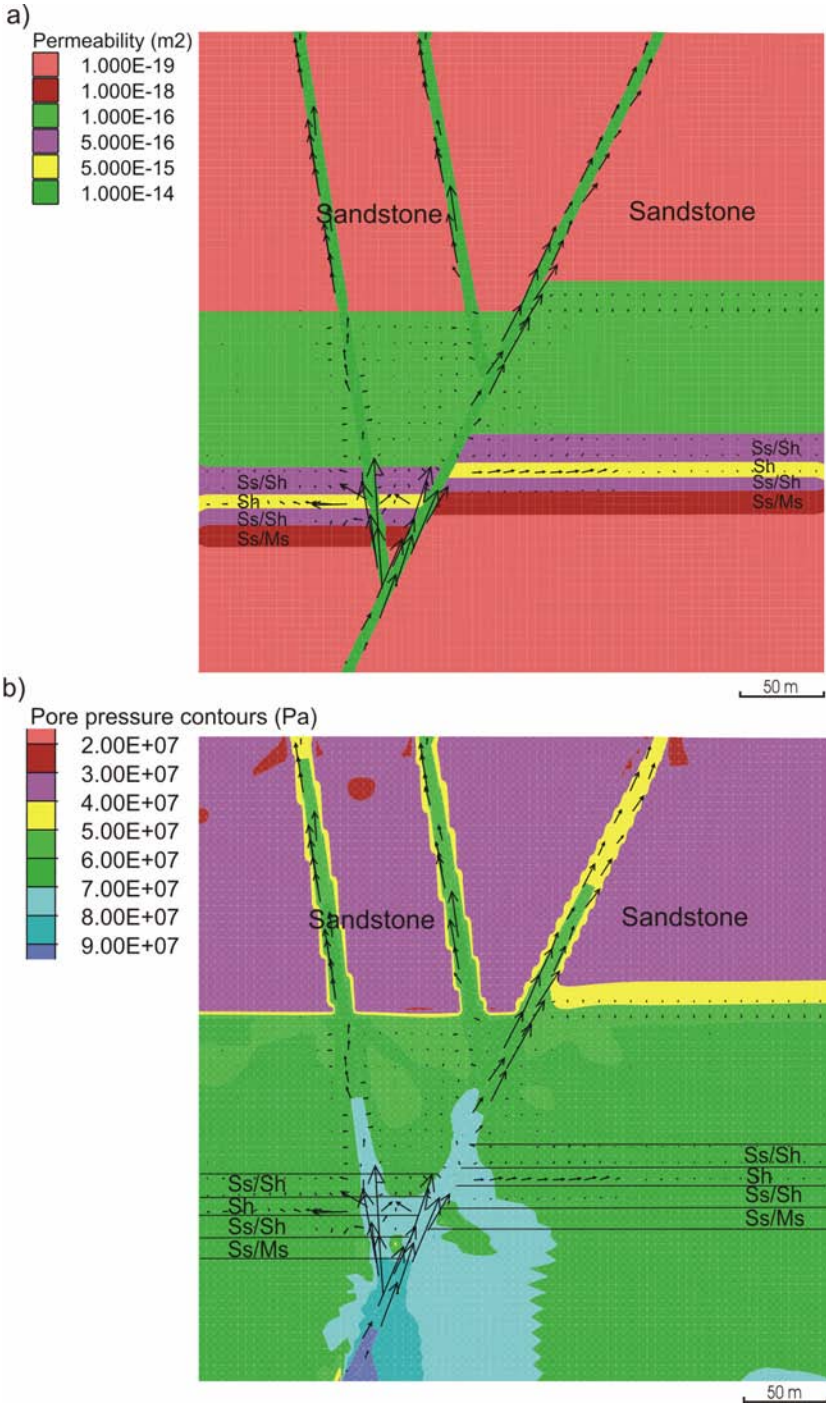
Fig. 4. 25 Model 2c at 1% deformation **a**) displaying permeability values and a strong Darcy fluid flow focussing within the fault zones. Lateral flow is evident within the shale layers, and **b**) plot of pore pressure contours and Darcy fluid flow vectors, displaying strong flow within the faults and minor lateral flow in the shale layers.
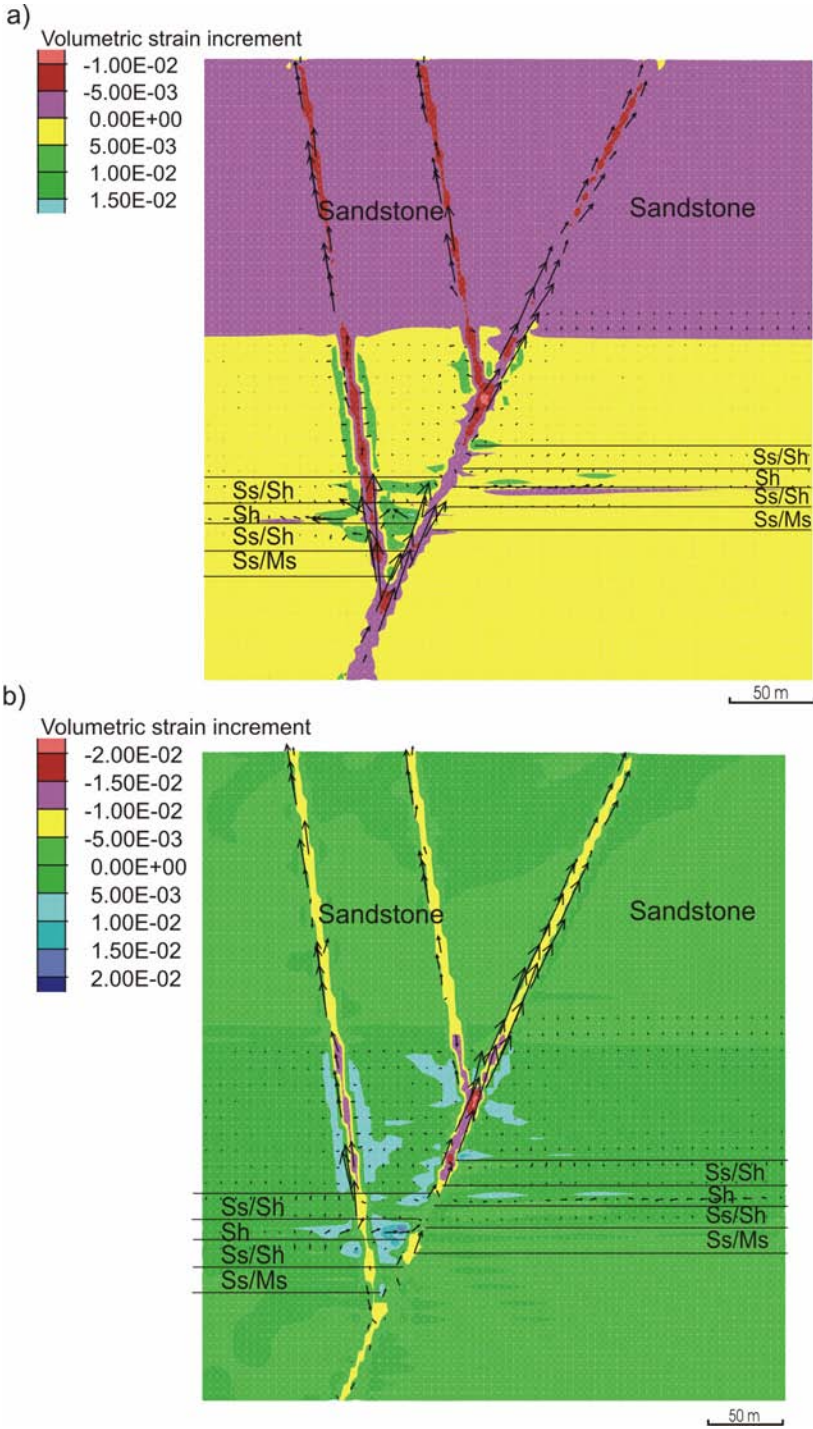
Fig. 4.26 Model 2c at **a**) 1% deformation, displaying volumetric strain (dilation) and a strong Darcy fluid flow focussing within the fault zones and towards dilatant areas in particular near fault intersections **b**) 5% deformation, plot of volumetric strain (dilation) and Darcy fluid flow vectors, displaying strong flow within the faults and lateral flow into the shale layers.

4.8.6.   Model 2d (contraction, high permeability shale, low permeability sandstone, with overpressure and yield permeability)

In an attempt to simulate hydrofracturing and resultant permeability increase in the shale units, an additional function was applied to this model which increased the permeability as a function of the plastic state of the material (i.e. as material reaches a yield state, shear or tensile failure, the permeability of the material at that point is increased by 10% from its original value, and returning or retaining its original value when not at yield). This function was to simulate the process of failure and increased permeability due to hydrofracturing, as proposed by Broadbent (1999). In early stages of compression (3% shortening) fluid flow is mainly driven upwards from the base of the more permeable fault structures, however downward migration of fluids is noted around the mid region of the model and within the faults (Fig. 4.27a), and this appears to be primarily driven by a localised decrease in pore pressure and dilatant effects (Fig. 4.27b). Fluid flow is focussed towards areas of dilation in the shale unit near the intersection of the main fault and the left branching fault, and these areas correspond to an increase in permeability due to failure (Fig. 4.28a). These areas display tensile failure, and due to the increase in permeability have focused much of the fluid flow within the model. As deformation progresses (5% shortening) fluid flow intensifies in this region as a result of pore pressure decreases and dilatant effects (Fig. 4.28b). Fluid flow within the shale layer is limited outside this region, and as a result of the yield function applied, the permeability of the shale unit remains one order of magnitude less

than that of the fault, hence, fluid remains focussed mainly within the fault zones. At later stages of contraction (7% shortening) similar results are apparent, with further dilatant effects driving fluid towards areas of failure and some localised contraction due to increasing shear strain (Fig. 4.29). Similar to Model 2c, the results of this model permit interpretations of focussed mineralisation in the shale units close to the faults.

In summary, results from Model 2 indicate that overpressure aids in upward migration of fluids within the more permeable faults, and potentially stimulates hydrofracturing within the shale units. To have any significant fluid flow within the shales, they must have permeabilities close to or the same as the faults. Addition of a 'yield function' to increase permeability within the model allows tensile failure and increased permeability within the shale unit, however, fluid is primarily drawn from the shale units towards the faults in most cases. This scenario also limits upward migrating fluids from deeper basinal horizons or basement material from entering the shale units, so ore genesis models using this scenario would have to source metals and sulphur from above. However, local areas between branching faults that display strong dilational characteristics may provide limited access to shales for deep seated mineralising fluids. Raised issues on permeability paths, their geometry, and their influence on grade distributions will be further addressed with 3D numerical models in the next chapter.
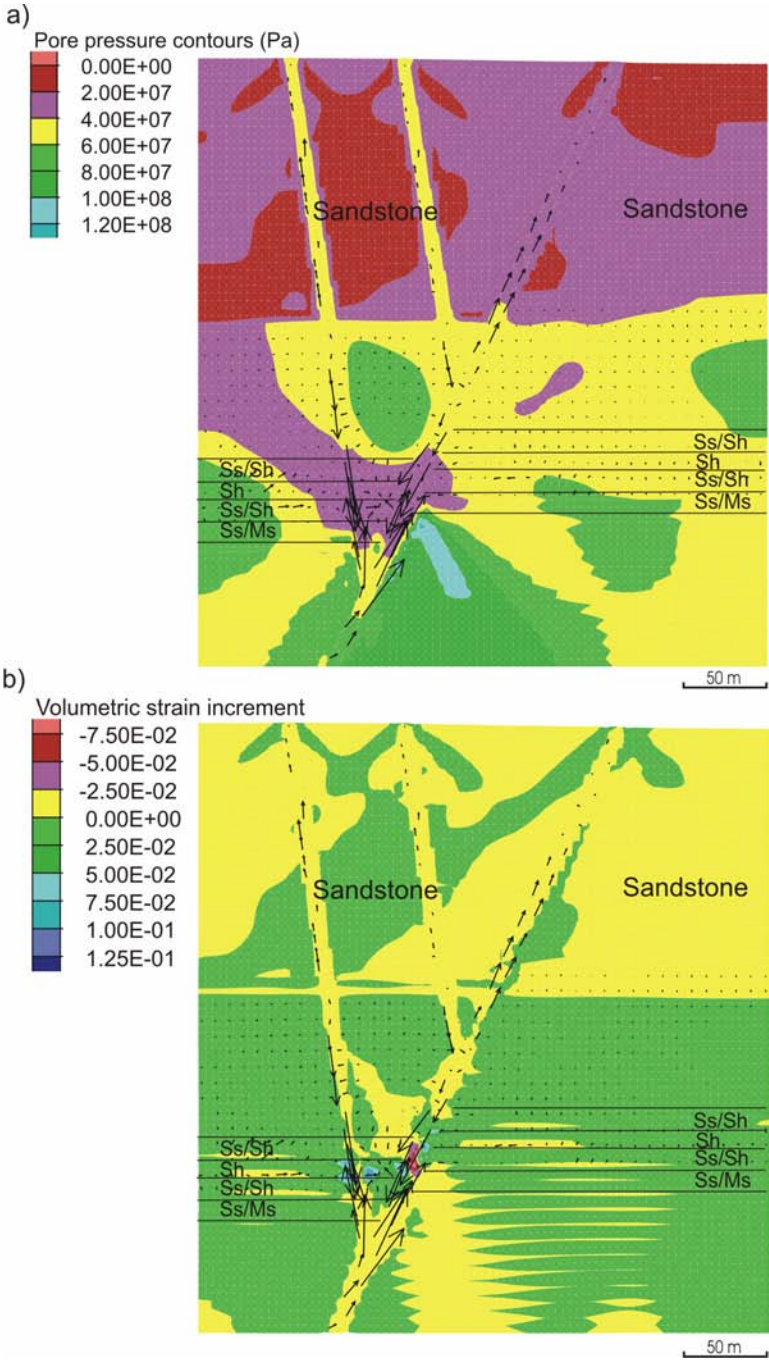
Fig. 4.27 Model 2d at 3% deformation a) displaying pore pressure contours and a strong Darcy fluid flow focussing within the fault zones and towards localised areas of pore pressure decrease b) plot of volumetric strain (dilation) and Darcy fluid flow vectors, displaying strong flow within the faults and focussing towards dilatant areas near fault and stratigraphic intersections of the ore zone.
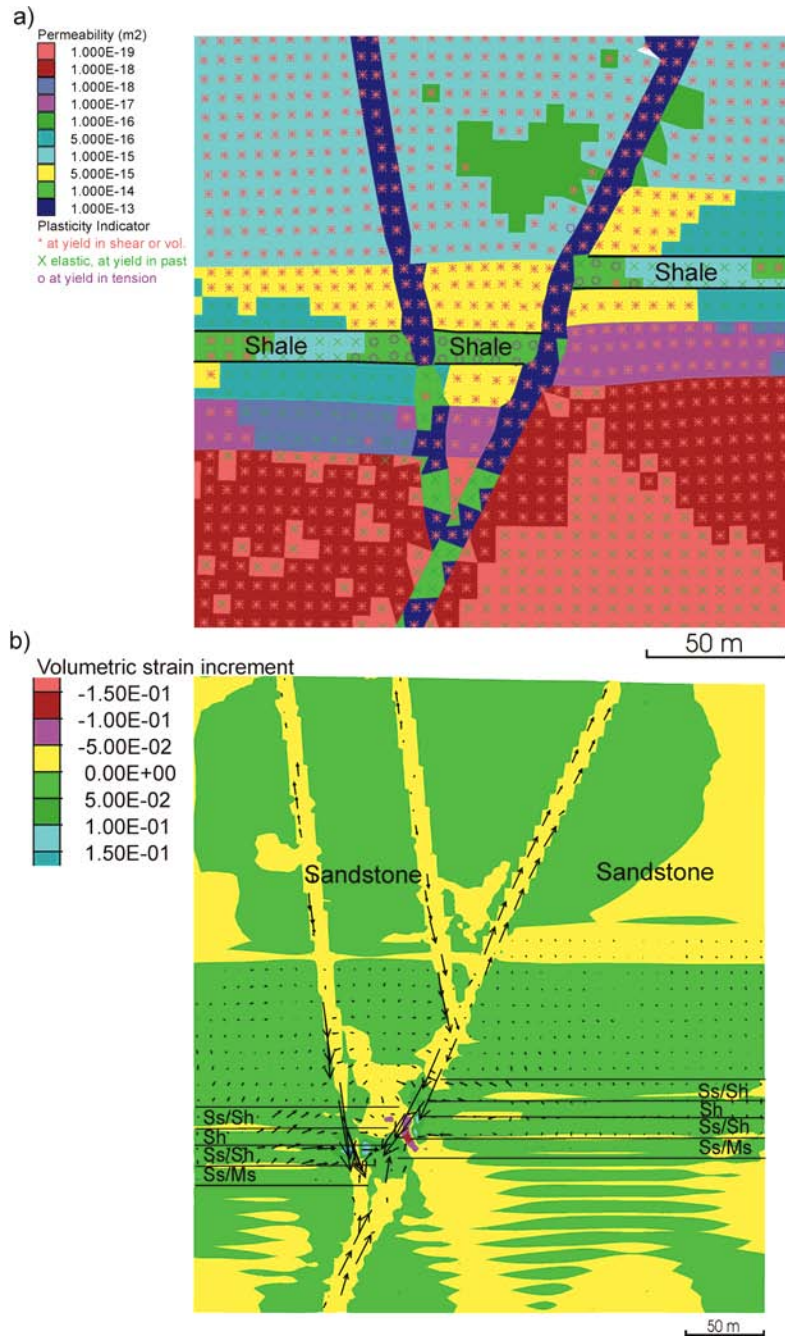
Fig. 4.28 Model 2d at a) 3% deformation, displaying permeability values and yield status or plasticity indicators. As a result of the applied yield function tensile failure is predominantly found in the shale layers (indicated by purple circles) and displaying high permeability values b) 5% deformation, plot of volumetric strain (dilation) and Darcy fluid flow vectors, displaying strong flow within the faults and focussing towards dilatant areas near fault and stratigraphic intersections of the ore zone, with strong fluid flow towards the fault notable within the shale layers.
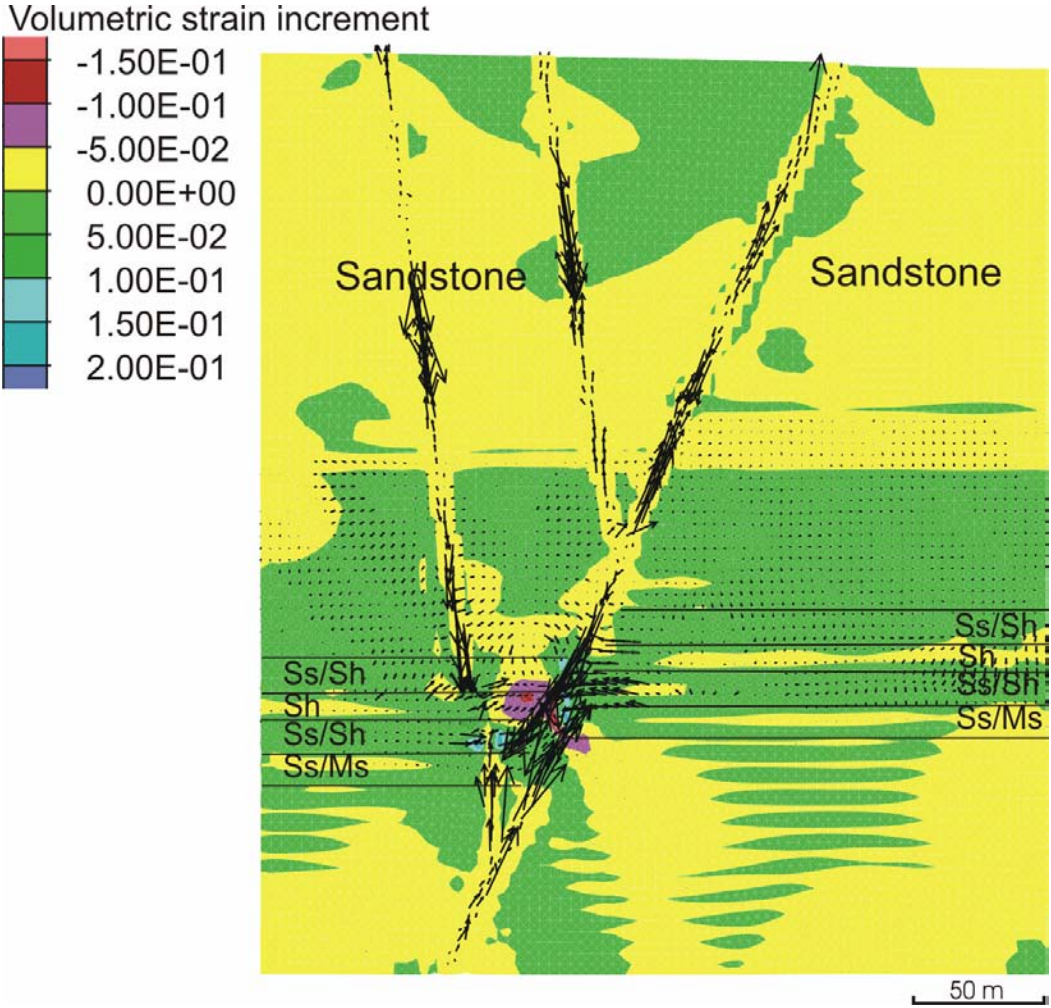
Fig. 4.29 Model 2d at 7% deformation displaying volumetric strain (dilation) and Darcy fluid flow vectors. Strong flow is evident within the faults and focussing towards dilatant areas near fault and stratigraphic intersections of the ore zone.

4.9.   Discussion and conclusions

Interpretation of the 3D structural model for Century suggests that there is a link between the regional and local scale NE trending structures, which relates to mineralisation. In particular, the regional faults contain vein type deposits (e.g. Silver King deposit) that preserve syn-tectonic breccia hosted mineralisation. Hence, proving that some of these structures intersect the Century deposit supports models for syn-tectonic mineralisation or models of remobilisation of earlier ores during the Isan Orogeny. However, these faults also show relationships to both sedimentary thickness variations and ore grades in Century, raising the possibility that they were active early and contributed to syn-sedimentary mineralisation. Interpretation of the TRF as a conduit for mineralisation (Broadbent, et al., 1998) was largely based on grade distribution data. We cannot discount the contribution of TRF fault to the ore system; however, this structure may have been more significant after basin inversion at Century, and as a consequence the general trends of Pb and Zn might be the final product of a more complex hydrothermal history in which the reactivation of faults within the deposit may have changed the original configuration of metal distributions. Zn grades and also thickness variation within Unit 200 have not been influenced by NW faults. Thus, NW faults branching from the TRF may have played only a minor role in ore genetic processes and more likely, if they contributed to the metal budget, they did so during later stages of Isan deformation as Broadbent (1999) suggests. This would explain why within Unit 200 the Zn grades do not seem to be influenced by these potentially later structures. Pb grades seem to be correlated with NE structures, but

overall the distribution is pointing to at least some influence of later NW structures. The consequence of these findings enhances our understanding of possible genetic relationships of the Century deposit and the Lawn Hill mineral field. We favour a model that envisages the emplacement of Zn and Pb early (syngenetic) as NE structures have been demonstrated to control thickness variation and grade distributions across the deposit, in agreement with the structural interpretation and available seismic profiles drawn in the northern part of the Lawn Hill Platform, which demonstrates that NE growth faults are regionally distributed. A model that additional syntectonic Pb or/and remobilisation of early Zn-Pb is also feasible. Late diagenetic to syntectonic emplacement models do not represent a single solution that fully explains our interpretation the results of the 3D model.

To test our remaining uncertainties, numerical simulations of the subsurface models (diagenetic, syntectonic) were undertaken. In normal circumstances sedimentary sequences have a reasonably well-defined variation in permeability, and shale is considered one of the least permeable units (e.g. Dullien, 1979). Our model results indicate that for fluid to permeate into shale sequences we require permeability values of the shale unit to be close to that of in-situ faults and much greater than surrounding sedimentary packages. Therefore, permeability is the primary factor controlling fluid flow and potential sites of ore deposition. The main observation from the extension models is that during extension, fluid from the surrounding sediments and the fault display extensive lateral migration into the shale units if the shale units are assigned high permeabilities. It is thus possible that migration of fluids along subsurface shale

units is mechanically feasible during extensional deformation and may provide the fluid pathways for stratiform diagenetic mineralisation.

Results from the models using fully compacted sediments indicate that overpressure is an additional process that aids in upward migration of fluids within the more permeable faults, and acts as a precursor to hydrofracturing within the shale units. However, the permeability of the shale must be at least $1/10^{th}$ that of the faults to provide any significant fluid flow through shale. Addition of a 'yield function' to increase permeability within the model allows tensile failure and increased permeability within the shale unit; however, fluid is primarily drawn from the shale units towards the fault in most cases. Overpressurisation may provide a process that induces hydrofracturing within the shale units; hence increasing permeability. This deformation induced permeability has the potential to focus fluids into these units; however, as shown by the modelling results these areas would be preferentially located close to the faults, therefore limiting any significant lateral fluid flow. Most of the fluids will then be preferentially driven in and through the fault domain. Thus, even with shale permeability set at unrealistically high values, this scenario works best for mineralisation proximal to faults, and might not be so useful to explain the lateral extent of primary Century mineralisation.

Revisiting the four modelling questions posed earlier, the pathways that controlled the location of favourable sites for mineralisation appear to be two-fold. In an extensional regime, normal reactivation of faults may provide localisation of fluids that have the potential to migrate laterally along more permeable sedimentary units, and during a compressional regime faults appear to be the main fluid conduits, with less

lateral migration of mineralising brines. It appears that both tectonic regimes are suitable for forms of mineralisation styles, however lateral flow is primarily favoured by extension. During compression, overpressurisation appears to have a strong influence over upward fluid flow and particularly tensile failure within the shale units, although this is spatially associated with faults, hence limiting lateral flow.

To conclude, it is apparent that we require either extremely permeable shale units in comparison to sandstones during early sedimentation, to contribute towards a subsurface replacive origin for mineralisation. More likely is the potential for significant failure within the shale units as a driving force for dilation and fluid flow focussing, as secondary porosity has less of an influence on transferring fluids laterally within the mineralised units of the Century deposit. We therefore conclude that a subsurface replacive origin for all the mineralisation is less likely than a syngenetic model with subsequent syntectonic remobilisation.